Eur. Phys. J. D (2014) 68: 348
DOI: 10.1140/epjd/e2014-50414-x

THE EUROPEAN PHYSICAL JOURNAL D

Colloquium

Laser selective spectromicroscopy of myriad single molecules: tool for far-field multicolour materials nanodiagnostics

Andrei Naumov[1,2,a,b], Ivan Yu. Eremchev[1], and Aleksei A. Gorshelev[1]

[1] Institute for Spectroscopy of the Russian Academy of Sciences, 142190 Troitsk, Moscow, Russia
[2] Moscow State Pedagogical University, 119991 Moscow, Russia

Received 28 May 2014 / Received in final form 2 August 2014
Published online 17 November 2014 – © EDP Sciences, Società Italiana di Fisica, Springer-Verlag 2014

Abstract. In this Colloquium, we discuss the main principles, achievements and perspectives in the field of highly parallel luminescence spectroscopy and imaging of single molecules (SM) in transparent solids. Special attention will be given to SM detection at low temperatures, where ultranarrow and bright zero-phonon lines (ZPL) of emitting centres are achievable for observation. Frequency of ZPL can be used as an additional property for separation of multiple SM images within diffraction limited volume, thus realising "multicolour" super-resolution microscopy. The extreme sensitivity of ZPL parameters to SM local environment allows application of SM spectromicroscopy for the study of structure and dynamics of doped solids on the nanometre scale. We show that the way to "bridge" the accidental rare events detected by SM probes to general material properties is a statistical analysis of spectral-spatial data obtained by a separated detection of all effectively fluorescing dye centres in a bulk sample. First experimental realisation of three-dimensional phononless luminescence SM spectromicroscopy with modification of SM point-spread function is demonstrated.

1 Introduction

Laser spectroscopy and imaging of single fluorescent molecules in transparent solids is a relatively young but already very powerful field of science. The first measurements of absorption and fluorescence excitation spectra of single molecules (SM) in polycrystalline matrices at low temperatures were realised in 1989 [1] and 1990 [2], correspondingly. Having joined soon after with luminescence microscopy and other related techniques, single-molecule spectroscopy (SMS) has quickly expanded to various emitting nano-objects (molecular complexes, nanocrystals, quantum dots, nanoholes, biological nano-objects, emitting sites in polymers and complex media, single ions and defects in inorganic solids, metallic nanoparticles, hybrid nano-objects). During the past 25 years, single-molecule spectroscopy and imaging (we will call this field on the whole as SM *spectromicroscopy*, SMSM) was intensively developed, and now is one of the most urgent multidisciplinary fields of science. SMSM methods became irreplaceable when resolving numerous problems of modern physics, physical chemistry, optics and spectroscopy, nano-optics and nanophotonics, material sciences and nanotechnologies, bio- and medical physics (see special issues [3–7]).

[a] e-mail: naumov@isan.troitsk.ru
[b] Web-page: www.single-molecule.ru

The incredible interest in SMSM can be attributed to at least several reasons:

(1) SMSM makes it possible to investigate the physical, chemical and functional properties of matter on the "smallest" level of SMs, including study of *intramolecular* processes (excited state dynamics, molecular vibrations and conformations, photoionization, Frank-Condon and Herzberg-Teller interactions, Auger recombination), direct observation of quantum processes (e.g. tunnelling, photon emission, luminescence blinking and bleaching) and connecting to macroscopic characteristics of the objects under study. It is important also that the SM system is a very convenient object for theoretical investigation and model calculation.
(2) Optical spectra of single dye centres embedded into condensed matter are very sensitive to local nanometre-scale environment. Thus single dye centres can be used as spectral nanoprobes for the study of *intermolecular* processes and interaction of probe molecules with surroundings (e.g. energy and charge transfer, electron-phonon coupling, spectral diffusion); and for the exploring of local dynamics of solids (e.g. elementary excitations of tunnelling and vibrational type, structural relaxations).
(3) SMSM is a basis of *far-field optical super-resolution microscopy* – an extremely "hot" and quickly growing

field of science and modern technology[1]. The main idea of the technique is based on the fact that the exact location (spatial coordinates) of a single point-like emitter can be found with nanometre-scale accuracy (much higher than the classical diffraction limit of far-field optics), which is limited only by the signal-to-noise ratio and the stability of a setup. This can be realised by computer analysis of SM luminescence images, detected by scanned confocal or wide-field luminescence microscope, taking into account its point-spread function (PSF). According recent research, even all three spatial coordinates can be restored by instrumental modification of PSF. In order to reconstruct a sample structure it is necessary to achieve a sufficient spatial density of chromophore labels without overlapping of their images. For this, one need to separate individual molecules located within the same diffraction-limited volume by an additional property. In the most popular techniques used so far (mainly in life sciences) sequential imaging of SM is applied with variable SM luminescence caused by random transitions between fluorescent and non-fluorescent states (blinking).

(4) There are various potential innovative applications of SMSM in nanosciences [8]. For example it is possible to develop controllable single photon light sources [9,10], to use SMs as extremely sensitive metrical nanoinstruments and nanosensors [11], to apply SMSM to quick DNA sequencing [12] and in flow cytometry [13].

The SMSM methods are especially informative at low (cryogenic) temperatures where zero-phonon lines (ZPL) of emitting centres are achievable for observation by excitation with narrowband laser light sources (see [14–19] and references therein). Unique properties of ZPLs substantially increase all the advances of impurity centre spectroscopy [20].

The phenomenon of ZPL, which corresponds to a purely electronic transition of an impurity and is usually considered as the optical analog of the Mössbauer line, was intensively studied during the last semi-century. Research in this area started from discovery of the Shpol'skii effect; followed by the discovery and theoretical understanding of the nature of ZPL, then by the discovery and development of selective laser spectroscopy techniques – laser fluorescence line narrowing, persistent spectral hole-burning, SMS, and finally by the development of fluorescence microscopy (detection of images and determination of SM coordinates with a sub-diffraction accuracy) of individual molecules in solid matrices.

The phenomenon of appearance of narrow ZPLs in doped solids is the basis for *truly multicolour far-field super-resolution microscopy* by single-molecule luminescence imaging. Actually, scanning through the *broad* inhomogeneous absorption spectral band yields the *extremely narrow* individual ZPLs and images of all fluorophores in the illuminated macroscopic volume of a sample [21,22]. Moreover *statistical analysis* of spectral-spatial data obtained for myriad SMs (ideally – all fluorescing SMs in a bulk sample) is a *sui generis* "bridge" between accidental rare events detected by SM probes and general material properties. This leads to the challenge of linking the distributions of SM spectral parameters with macroscopic photo-physical data.

In this Colloquium we discuss recent achievements in the field of phononless optical reconstruction single-molecule spectromicroscopy, its main problems and open questions, as well as perspectives and potential applications.

2 "Zero-phonon line as a keystone for high resolution spectroscopy"[2]

2.1 Spectroscopy of impurity centres

Electronic-vibration spectra of dye-centres (chromophore molecules) in transparent matrices contain valuable information about intra- and intermolecular processes in doped solids. Moreover, complex organic molecules being fixed in a rigid matrix are very suitable simplified objects for study, because of "freezing" of the majority of rotational and conformational degrees of freedom. This makes it easier to resolve both primal and inverse spectroscopic problems in molecular spectroscopy. At the same time electronic transitions of impurity chromophores are very sensitive to processes in local matrix surroundings, thus chromophore-matrix interactions give rise to complication in spectra. One of the most significant matrix influences is the effect of *inhomogeneous broadening*. The essence of this effect is a strong distribution of electronic transition frequencies of individual chromophores which are located in slightly different conditions in real solids. As a result the electronic-vibrational spectra are subjected to strong blurring even in the case of quite ordered molecular crystals. This effect was a long time a "bottleneck" that prevented full interpretation of spectra of dye-doped solids with complex structure.

2.2 Shpol'skii effect

The first essential step to resolving the inhomogeneous broadening problem was the discovery of the Shpol'skii effect in 1952 (see Ref. [23] on this subject). It was found that in a set of frozen solvents (linear n-alkanes) a quasi-linear thin structure originates in luminescence spectra of organic chromophores. The phononless nature of Shpol'skii spectra was clarified in a series of theoretical works [24–28] (see also [29–31]) as a result of specific transitions in a molecule, which arise without creation/annihilation of matrix phonons, i.e. without changing of the crystal state. Such transitions lead to the appearance of narrow *zero-phonon lines*, whereas transitions

[1] The Nobel Prize in Chemistry 2014 was awarded jointly to E. Betzig, S.W. Hell and W.E. Moerner for the development of super-resolved fluorescence microscopy [S.W. Hell, Far-Field Optical Nanoscopy, Science **316**, 1153 (2007)].

[2] This very meaningful definition was done by one of the founder of laser selective impurity center spectroscopy field of sciences, Prof. K.K. Rebane.

which involve participation of phonons cause the appearance of broad *phonon sidebands* (PSB). In Shpol'skii matrices the probability of phononless transitions is high and inhomogeneous broadening is quite small, thus relatively narrow quasi-linear electronic-vibrational spectra can be observed in experiment even upon non-laser excitation. The subsequent decades have given rise to intensive study of quasi-linear spectra for various chromophore molecules in Shpol'skii matrices. The resolved vibrational structure of Shpol'skii spectra gives the opportunity to find frequencies of molecular vibrations of the ground and excited states, and investigate photophysical and photochemical properties of complex organic molecules.

2.3 Laser selective spectroscopy

The main disadvantage of spectral techniques based on the Shpol'skii effect was the strong limitation of dopant/matrix materials suitable for the observation of quasi-linear spectra. In the majority of disordered solids, the width of the inhomogeneous absorption band γ_{inhom} can reach several hundred cm^{-1}, thus preventing observation of resolved electronic-vibration spectra.

Soon after the first description of ZPL as an optical analogue of Mössbauer effect, it became clear that the influence of inhomogeneous broadening can be eliminated via monochromatic excitation. For example, already in early works it was found that luminescence spectra of impurity ions in inorganic glasses are narrowed upon excitation with the relatively narrow lines of a mercury lamp [32].

The cardinal development of impurity centre spectroscopy occurred after the development of truly monochromatic laser light sources. In reference [33] the inhomogeneous broadening of the R-line in a ruby crystal was removed and a ZPL was detected under monochromatic excitation. Wherein the possibility of observing ZPL (and even the existence of ZPL) in highly disordered solids was debated for a long time.

In 1972, Personov with colleagues have reported the appearance of a fine ZPL-based structure in the electronic-vibration spectra of dye-molecules in a highly disordered matrix (organic glass) upon monochromatic laser excitation [34,35]. Moreover they concluded that this effect is general to almost any dye-doped solids, including highly disordered organic glasses, polymers, and biological media. This method was called *laser-induced fluorescence line-narrowing* (FLN), in some publications as *the Personov effect* [36]. Two years after FLN discovery, another important milestone was reached in the development of dye-doped solids selective spectroscopy. It was revealed that the absorption spectra of some doped solids can be modified by laser illumination, because of photochemical or photophysical transformations of the dopant molecules. Such changes lead to the appearance of a narrow "gap" in the absorption spectra, which corresponds to ZPLs position of selectively transformed molecules. Thus the method of *persistent spectral hole-burning* (HB) was developed [37,38].

Both FLN and HB techniques have gained incredible popularity and were used intensively for studying the nature of various inter- and intramolecular processes in a wide range of doped solids, for investigation of mechanisms of dye-matrix interactions, internal dynamics of matrices and quantum-size effects. Based on FLN and HB, numerous methods and approaches were developed for studying temperature dependences, influence of thermal cycling, external electric and magnetic fields, pressure dependences, polarisation dependences, multiphoton processes, and time-domain processes. HB technique was also involved in the development of multidimensional holography [39] and investigation of slow light phenomenon [40]. Laser selective spectroscopy remains in widespread use for studying a broad range of doped condensed matters and fluorescence dyes of different structure and chemical composition: crystals, glasses and polymers [41,42], rare gas matrices [43], nanoporous materials [44], quantum dots [45], *J*-aggregates [46], nanodiamonds [47,48], nanostructures [49], proteins [50], light-harvesting complexes [51,52], and bioanalytical species [53].

2.4 Single-molecule spectroscopy and imaging: short timeline

In spite of their high spectral selectivity, FLN and HB address a large number of chromophores, thus averaging spectral data over a sub-ensemble of spatially distributed impurities. For this reason, during 1960–1980 scientists can only ponder over the possibility of single-molecule detection. SMs in a solid matrix were detected for the first time in 1989 [1] by absorption spectroscopy, and soon after in 1990 [2] by detection of fluorescence excitation spectrum. The first measurement of finely-resolved electronic-vibration luminescence spectrum of SMs in crystalline matrix was done in 1994 [54]. The first fluorescence low-temperature imaging of SMs in solids with a 2D-detector was reported in 1994 as well [55], showing the possibility of highly parallel measurements of SM coordinates and spectra.

All these pioneering experiments were performed at cryogenic temperatures, viz. ZPLs of SMs were detected. One can suppose that this success was based on the unique properties of ZPL (brightness and high spectral selectivity). These works started worldwide SMS-studies of structure and dynamics of molecules, amorphous media, solids and nanostructures with ultra-high spatial, temporal and spectral resolutions [3–7].

The whetting of scientific "appetite" for SMSM occurred due to, at least, several reasons:

(i) Progress in modern optics, spectroscopy and related technologies.
(ii) Development of highly sensitive matrix detectors (CCD- and CMOS-cameras).
(iii) Rapid growth of power of personal computer systems.
(iv) Progress in chemical and novel material sciences.

In 1993–1994 SMS has been extended to high temperature ambient conditions with near-field [56–58] and in

1994–1996 with far-field [59,60] optical microscopy. This was the beginning of SMS applications in huge areas of biophysics and life sciences [61]. In this field the diagnostics of ultrafast phenomena is of special interest, and to date such SMS technique has been realised [62].

In 1996–1998 it was experimentally shown that the accuracy of SM lateral coordinates reconstructed by computer analysis of SM luminescence images is not restricted by the Abbe diffraction limit of far-field optics, but depends only on the signal-to-noise ratio during measurements and can reach a few tens of nanometres [63,64]. Hereafter researches have shown that by taking into account the SM point-spread function, precise SM images analysis can restore coordinates with even sub-nanometre accuracy [65].

The technology breakthrough in SMSM in the second half of 2000s was the development of *wide-field luminescence microscopy with real-time SM images processing* which gives sub-diffraction reconstruction of SM spatial coordinates. In 2006, a set of far-field super-resolution optical microscopy techniques were developed based on the reconstruction of spatial positions of numerous single probe molecules: stochastic optical reconstruction microscopy (STORM) [66] and photoactivation localisation microscopy (PALM) [67]. These super-resolution techniques have found a broad application in science (especially, in biophysics and life sciences), gave rise to developments in numerous subfields and innovative optical devices have already entered mass-production.

Modern adaptive optical technologies opened up the possibility of manipulating the SM emission wavefront, modifying the SM point-spread function on-demand. On this basis, the techniques of double-helix PSF (DH-PSF) [68] in 2009, and recently bisected pupil PSF (BSPPSF) [69] were developed for SM imaging. These techniques open up avenues for three-dimensional imaging with resolution beyond the diffraction limit.

ZPL-phenomenon was also used as a basis for "truly multicolour" super-resolution microscopy. In 2009 the technique for phononless luminescence optical reconstruction single-molecule spectromicroscopy (PLORSM) [22] was developed, which is based on sequential-parallel detection of phononless luminescence images and ZPLs for nearly all illuminated single molecules in a bulk sample. At cryogenic temperatures, narrow ZPLs of single probe fluorophores can be excited in a controlled way by frequency-tuning of the narrowband excitation laser within the broad inhomogeneous absorption spectral band. The number of resolved SMs within a diffraction-limited spot depends on the ratio $\gamma_{\text{inhom}}/\gamma_{\text{ZPL}}$, which at cryogenic temperatures in disordered solids, is of the order of 10^5–10^6 (where γ_{inhom} is a width of inhomogeneous absorption spectral band, γ_{ZPL} is a homogeneous ZPL width). Thus, the ZPL frequency can be used as an additional property for separation of SM images, which one can consider as the "colour" of a SM. In addition, the huge peak intensity of ZPL under narrowband excitation allows high-precision reconstruction of SM coordinates with small exposition times. Thereby, the hyperspectral nanodiagnostics (or, in other words, highly selective spectral "nanotomography") of doped solids can be realised for material science applications.

2.5 Zero-phonon line properties

Since pioneering research in the field, the nature of ZPL is discussed in terms of electron-phonon coupling [24–31]. Later on the theory was generalised to electron-phonon couplings of any strength as well as phonon localisation (see [70–72], books [73,74] and references therein). Advances in SMS stimulated a series of theoretical works, which clarify the microscopic nature of SM-matrix interaction, including interaction with low-energy excitations of both vibrational and tunnelling type [73–76]. Interestingly, many aspects of the theories developed so far have found a use for spectroscopy of semiconductor quantum dots in solid matrices when describing exciton-phonon coupling [77–79]. Below we restate several frequently used equations which describe the parameters of ZPLs in doped solids.

The relation between the integrated intensity of the ZPL and the total intensity of the single vibrational spectral band (called the Debye-Waller factor) is determined by linear electron-phonon coupling and depends on the temperature:

$$\alpha_{\text{DW}}(T) = \frac{I_{\text{ZPL}}}{I_{\text{ZPL}} + I_{\text{PSB}}} = \exp\left[-\int_0^\infty g(\nu)\,(2\,n(\nu)+1)d\nu\right], \quad (1)$$

where $n(\nu) = 1/[(\exp(h\nu/kT) - 1]$ is the Bose factor, $g(\nu)$ is the density of coupled phonon states of the system. Thus the ZPL intensity transfers to the PSB intensity with increasing temperature, while the integrated intensity of the vibronic band does not depend on temperature. As it was found in previous studies with ensemble-averaged techniques, in general, I_{ZPL} and α_{DW} can depend on other system parameters (e.g. excitation wavelength [80]). It means that single molecules (which are chemically the same) in different places of the matrix can possess varied Debye-Waller factors.

Numerous studies (see, e.g., [18] and references therein) have shown that the homogeneous ZPL width Γ_{ZPL} in the temperature range well below the melting/vitrification temperatures is determined in general by three main contributions:

$$\Gamma_{\text{ZPL}}(T) = \Gamma_0 + \Delta\Gamma_{\text{e-tunn}}(T, t_m) + \Delta\Gamma_{\text{e-phon}}(T), \quad (2)$$

where Γ_0 is the natural linewidth of ZPL; $\Delta\Gamma_{\text{e-tunn}}(T, t_m)$ is the ZPL broadening caused by the interaction of electronic transitions in impurity molecules with tunnelling excitations in the matrix, which depend on the total time of measurement t_m; and $\Delta\Gamma_{\text{e-phon}}(T)$ is the ZPL broadening caused by the interaction of impurity molecules with vibrational excitations (electron-phonon interaction).

Meanwhile the electronic transition frequency ω (frequency position of ZPL) of the chromophore molecule also depends on the temperature T and time of observation t_m:

$$\omega\left(T,t_m\right)=\omega_0+\Delta\omega_{\text{e-tunn}}\left(T,t_m\right)+\Delta\omega_{\text{e-phon}}\left(T\right). \quad (3)$$

This equation takes into account: (i) The static shift of ZPL, ω_0, which determines the "true" position of ZPL within the inhomogeneous absorption band, and depends on particular incorporation of the SM into matrix structure, on the local surrounding structure, local elastic and electric fields. (ii) The ZPL frequency shift $\Delta\omega_{\text{e-tunn}}$ due to interaction of SM with tunnelling type excitations. This interaction gives rise to spectral diffusion resulting in the SM ZPL frequency jumps. (iii) The frequency shift of ZPL $\Delta\omega_{\text{e-phon}}$ induced by electron-phonon interaction.

The natural linewidth Γ_0 is determined by the excited-state lifetime of the molecule. As recent research has shown, this parameter depends on the matrix parameters, such as the refraction index [81,82]. The influence of local surroundings on the value of Γ_0 becomes pronounced in the case of interaction of molecules with nanostructures, e.g. Purcell effect when the molecule is located in a microcavity or interacts with plasmonic nanomaterials [83–86].

Considering the interaction of a SM electronic transition with low-energy excitations of the tunnelling type, one usually uses the standard model of low-temperature glasses which is based on the tunnelling two-level systems (TLS) and stochastic sudden-jumps models [87–89]. Within this approach the ZPL frequency for each molecule is determined by independent tunnelling transitions in all nearby TLSs [75]:

$$\Delta\omega_{\text{e-tunn}}\left(T,t_m\right)=\sum_j\zeta_j\left(t\right)\,\upsilon_j\ \text{ where }\ \upsilon_j=2\pi\Lambda\frac{A_j}{E_j}\frac{\varepsilon_j}{r_j^3}. \quad (4)$$

Here $\zeta_j(t)$ is a stochastic variable equal to -1 or $+1$, when the jth TLS is in its ground or in its excited state, respectively; Λ is the TLS-chromophore coupling constant; A_j, E_j, and ε_j are the asymmetry, energy, and orientation parameter of the jth TLS, respectively; and r_j is the TLS-chromophore distance.

The dependence of ZPL broadening due to chromophore-TLS interaction within the standard model of low-temperature glasses is defined in general as follows [90,91]:

$$\Delta\Gamma_{\text{e-tunn}}\left(T,t_m\right)\sim T^{\alpha}\,\ln\left(t_m\right),\quad \text{where}\quad 1\leqslant\alpha<2. \quad (5)$$

In order to describe electron-phonon interaction, one needs to take into account both Debye phonon states, local phonons, as well as quasi localised low-frequency vibrational modes (which are inherent to strongly disordered solids [92]).

The spectral line broadening of an impurity centre, caused by the quadratic interaction of an electronic transition with the phonon excitation spectrum, can generally be described (for any electron-phonon coupling strength) by the expression [73]:

$$\Delta\Gamma_{\text{e-phon}}\left(T\right)=\frac{1}{4\pi}\int_0^{\infty}\mathrm{d}\nu\ln\left\{1+4n\left(\nu\right)\left[n\left(\nu\right)+1\right]\times W^2 g_{(0)}\left(\nu\right)g_{(1)}\left(\nu\right)\right\}, \quad (6)$$

where W is the constant of quadratic electron-phonon coupling; $g_{(0)}\left(\nu\right)$, $g_{(1)}\left(\nu\right)$ are phonon densities of states in the ground and excited states of the chromophore.

The intensity of ZPL is in close connection with the luminescence quantum yield and is defined by various properties of the system. With SMS methods one can look inside different processes, which determine the luminescence yield and ZPL intensity. For example an important question is the study of SM absorption and ways of controlling this process. The experiments [93] have shown that strong extinction of a laser beam by a SM is observable at some conditions (even full extinction is possible using near-field excitation). I_{ZPL} depends on the value of Debye-Waller factor (Eq. (1)) i.e. on the phonon density of states and their coupling with dopants. Local environment can also strongly affect I_{ZPL}, especially when the SM interacts with various nanostructures. For example, luminescence enhancement by several orders of magnitude is possible due to the Purcell effect [85] and with the use of optical nanoantennas [83,84].

ZPL width and amplitude depend also on the laser excitation intensity P_{LAS}:

$$\Gamma_{\text{ZPL}}\left(P_{\text{LAS}}\right)=\Gamma_{\text{ZPL}}\left(0\right)\sqrt{1+P_{\text{LAS}}/P_S}, \quad (7)$$

$$I_{\text{ZPL}}\left(P_{\text{LAS}}\right)=I_{\max}^{\infty}\frac{P_{\text{LAS}}/P_S}{1+P_{\text{LAS}}/P_S} \quad (8)$$

where P_S is saturation intensity, $I_{\max}^{\infty}$ is the ZPL fully saturated emission rate, $\Gamma_{\text{ZPL}}\left(0\right)$ is the unsaturated ZPL spectral width.

Note that low P_S values usually correspond to a lateral orientation of the SM transition dipole moment. In fact, the relative orientations of the excitation light polarisation and the SM dipole moment influence strongly the observable ZPL luminescence [14,94]:

$$I_{\text{ZPL}}\cong\left(\mathbf{d}\,\mathbf{E_L}\right)^2=d^2E_L^2\sin^2\theta_d\cos^2\left(\varphi_d-\varphi_L\right), \quad (9)$$

where $\mathbf{d}$ is transition electric dipole moment of the SM; $\mathbf{E_L}$ is electric field vector of the excitation laser light; θ_d, φ_d, φ_L are angles between $\mathbf{d}$-vector and z-axis, xy-projection of $\mathbf{d}$-vector and x-axis, and $\mathbf{E_L}$ vector and x-axis (x, y, z-axes are some chosen Cartesian coordinate system, in which $\mathbf{E_L}$ is in the xy-plane). Thus I_{ZPL} depends strongly on the relative orientation of $\mathbf{d}$ and $\mathbf{E_L}$ vectors and this dependence is the basis of SM polarization spectroscopy [14,94,95].

Because of different $\mathbf{d}$-orientations of SMs relative to the microscope optical axis, the emitting dipole radiation pattern also influences the detected luminescence signal. This is especially important when the SM is located near the interface of two media with different refraction indexes [8]. Moreover, $\mathbf{d}$-orientation dependent SM radiation

pattern should be taken into account in the SM imaging techniques, when correct super-resolution reconstruction of SM coordinates is achieved only with proper PSF analysis [65]. Also this dependence can be used for more effective luminescence excitation by proper manipulation with laser beams, for example by preparing the light source with a high axial polarisation component [96].

Applying external electric or magnetic fields leads to the observation of Stark or Zeeman effect, respectively, which lead to ZPL frequency shift [14]:

$$\Delta\omega_{\text{field}} = -\left(\mathbf{\Delta}\mu \cdot \mathbf{F} + \mathbf{F}\,\chi\,\mathbf{F}\right), \tag{10}$$

where the first and second terms describe linear and quadratic effects, respectively; $\mathbf{\Delta}\mu$ is the change in electric (or magnetic) dipole moment of the molecule, $\mathbf{F}$ is field intensity, χ is the change in the electric (or magnetic) susceptibility tensor. Thus, a SM can be used as a very sensitive nanoprobe of local electric and magnetic fields [97–99].

3 Single molecule spectromicroscopy

3.1 Main principles

Several conditions should be satisfied in order to achieve SM detection:

(a) *"Bright" and photostable chromophore molecules,* with a sufficient length of excited state lifetime and low quantum yield of internal conversion (transition into long-lived triplet state). The processes of reversible transitions of the chromophore into radiationless "dark" or "grey" states (so called "blinking" [100–103]) play a very important role, as well as irreversible "bleaching". These processes can, in some cases, prevent proper SMSM experiments from being carried out, but in other cases can be the basis of specific techniques (e.g. STORM and PALM techniques [66,67]).

(b) *Low background and parasitic light contributions* to the detected signal (i.e. specific choice of dye-matrix pairs, chemical purity of the sample components and solvents, extreme cleaning of substrates, cuvettes and optical elements of the setup). When SM "guests" embedded into "host" solid matrix or liquid are being detected, the spectral properties of the "host" should be different: the absorption spectra of guest molecules and host condensed matter should not strongly overlap. Also in some cases radiationless intersystem crossing to host triplet state strongly diminishes SM emission efficiency [104].

(c) *Highly sensitive light detectors* with sensitivity capable of single photon counting, with quantum yield as high as possible, very low intrinsic dark and reading noises, broad range of exposure times, short "dead" times [105,106].

(d) *Optical elements with specific characteristics*: objectives with high numerical apertures, small aberrations. Filters with desired sharp-edged pass bands.

(e) *High mechanical stability* of optics-mechanical elements of the setup and high precision transmission units. This is especially important in the case of cryogenic experiments where transmission stage and objective are placed into the measuring chamber of a cryostat [107].

(f) *Specific algorithms and software* for fast data processing (SM image recognition and hyperspectral analysis); powerful computer systems for large data-flow processing and storage. This point is extremely important in the case of highly parallel detection of myriad SMs and further statistical data analysis. This quite sophisticated problem is closely related to the general multidisciplinary problem of pattern recognition and image processing, which is undergoing intensive development in astronomy, machine vision, etc. [108,109]. In relation to SMSM there are several open-source software packages for highly effective SM image processing for the STORM and PALM techniques [110,111], and also for the DHPSF technique [112].

(g) *Sine qua non is emission of only one SM per diffraction limited volume* (DLV) at a time with the selected exposure, or possibility to separate images of certain single molecules within DLV of a sample by some additional property. Primarily, it can be achieved by proper choice of dye concentration (Fig. 1a), by reducing the sample volume under study (thin films, sharp excitation light focusing with use of confocal excitation-detection scheme). However, if all molecules emit light simultaneously, the required concentration is "homeopathic" ($\sim$10 molecules per μm^3 for the visible range of wavelengths), that is not always suitable for the physical problem under study. For example, in super-resolution microscopy techniques based on reconstruction of numerous SMs positions, it is principally important to detect separately many emitters within DLV in order to restore the nanostructure of the sample. For resolving this problem there are several approaches.

The first (and the most popular [66]) one is using the blinking effect, intrinsic for many single molecular emitters. Each molecule in a sample is stochastically switching between emitting (on-) and non-emitting (off-) states. Thus one can select experimental conditions such dyes, concentration and exposure time, that at each time moment, only one SM per DLV is fluorescing (Fig. 1c). Making numerous sequential snapshots, one can detect separate images for the required number of SMs in order to restore the structure of the sample. The only problem is to make single emitters switchable. In most popular super-resolution techniques, the blinking of fluorescence chromophore labels attached to biological macromolecules is used. This blinking is caused by stochastic conformational changes of biological macromolecules, resulting in changes of the efficiency of nonradiating energy losses of emitters.

The second possibility to resolve simultaneously fluorescing SMs within DLV is the separation of their emission by some additional property, for example by

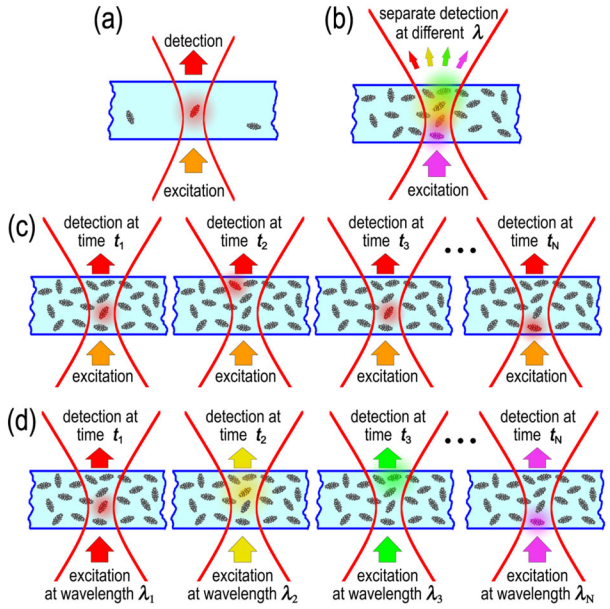

Fig. 1. An illustration of the principles of single-molecule spectromicroscopy. (a) Resolving of individual SMs within diffraction limited volume by extreme low dyes concentration. (b) Resolving of SMs by selective detection at different wavelengths. (c) Resolving of SMs by effect of stochastic blinking (switching) of molecules. (d) Resolving of SMs by selective narrowband excitation of different molecules at different wavelengths. Red lines show conventional borders of diffraction limit volumes.

the wavelength of emission. For this, one can dope the condensed matter with several sorts of dyes which emit light in different wavelength regions at the same excitation (Fig. 1b). Thus different molecules are detectable separately by sequential changing of special band-pass filters. In principle, this idea is very closely related to the concept of "Raman fingerprints".

Finally, another way to achieve a high concentration of resolved SMs is to use spectrally selective excitation. For this, one can use a wavelength tunable light source (e.g. tunable laser). Tuning of the laser frequency into resonance with the SM absorption line maximum allows controllable and deliberate excitation of different molecules within the same DLV (Fig. 1d). For the best realisation of this approach, the molecules should have homogeneous absorption spectra which are as narrow as possible, distributed over an inhomogeneous absorption band that is as broad as possible. Narrow ZPLs meet the conditions for this "multicolor" technique in the best possible way, because of an unprecedentedly high ratio between inhomogeneous and homogeneous bandwidths. This idea was for the first time realised in [22] and is the central subject of the present Colloquium paper.

3.2 Experimental methods

Up to the present time SMSM has been realised in spectroscopy and microscopy techniques (see e.g. [113–116]), most commonly used of which will be shortly discussed below.

3.2.1 Absorption spectroscopy

This technique was used in the pioneering work on SMS [1] and is in active current use. The main peculiarity of absorption methods is that the relatively weak signal has to be detected on the large background, thus it requires special experimental techniques like Stark-modulation, etc.

The high interest of SM absorption techniques is stimulated by their possible applications for the photothermal therapy and microscopy of non fluorescent samples. At present, absorption techniques are actively applied to single nano-objects of various nature: metal nanoparticles and nanoclusters, hybrid nano-objects. For example, in reference [117], the technique of absorption and scattering microscopy of single metal nanoparticles was realised on the basis of the photothermal method, which significantly improves the signal-to-noise ratio. In reference [118], SM imaging by optical absorption was performed, which significantly expands the range of objects that can be studied by SMSM, including samples which absorb light, but do not fluoresce. A new, prospective direction in this field is the development of hybrid nanoparticles which has optical properties that can be designed on-demand by numerical computation (e.g. FDTD-simulation of metal-organic nanoparticles [119]).

3.2.2 SM emission spectroscopy

When applied to SMS, classic luminescence spectroscopy is a powerful way to understand the microscopic nature of intramolecular interactions. By analogy to bulk spectroscopy (see e.g. [120,121]), vibrational analysis of the resolved luminescence spectra can be performed. Such analysis can give the parameters of Franck-Condon and Herzberg-Teller interactions, information about breaking of molecule symmetry due to matrix influence, and the values of molecular vibration frequencies (for examples of SM vibration identification (see Ref. [54]). In this way, the best results can be obtained at low temperatures, when the luminescence spectra consist of narrow ZPLs and are highly resolved. For this application one can also refer to a huge field of SM Raman spectroscopy, especially surface enhanced techniques, which have found a broad use in modern spectroscopy, plasmonics and related fields. In addition, multiphoton techniques are also applicable. One of the main advantages of emission spectroscopy is the possibility of spectrochemical identification and analysis of the light-emitting molecules.

3.2.3 Fluorescence excitation technique

Since pioneering works on SMS in 1989-90s it has become clear that fluorescence excitation technique yields a much higher signal-to-noise ratio when detecting single molecules [1,2]. In this technique, a SM fluorescence is excited by a narrowband light source at a wavelength within the SM absorption spectral band. Integrated

Stokes-shifted fluorescence of the SM is detected, while the excitation frequency is tuned over the SM absorption spectral band. The fluorescence excitation spectrum (dependence of integral luminescence on the excitation frequency) is the equivalent of an absorption spectrum, but exhibits much higher (in multiple orders of magnitude) signal-to-noise ratio. Fluorescence excitation spectroscopy became the most used technique for the SMS study of low-temperature doped solids, in particular, the study of low-temperature dynamics of disordered solids, such as glasses, polymers, defected polycrystalline samples (see [14–19] and references therein). Numerous impressing results in this field were obtained in studies of both organic dye molecules photophysics and low-temperature dynamics of disordered molecular systems (some of these results will be highlighted in Sect. 4 of this Colloquium). Moreover, the ZPL phenomenon was used as a basis for a new super-resolution far-field optical microscopy technique [21,22] which idea is discussed in Section 5 of this Colloquium.

3.2.4 Analysis of autocorrelation functions, blinking time traces and photon statistics

Since early SMS works, the study of temporal dynamics of SM emission was a source of information about quantum emitters. For example, observation of detected photon antibunching by analysis of the correlation function was (and remains currently) the best way to confirm the individual character of an emitter, because a SM cannot emit two photons at the same moment [122]. The correlation function is also a source of information about intersystem crossing, transition into "dark" states and other processes.

The statistical analysis of SM fluorescence intermittency over a long time period gives information about the microscopic nature of "dark" and "grey" states of single emitters, in particular about the roles of photo-oxidation, phototransformation, photo-ionisation, triplet states and energy transfer in SM luminescence blinking and bleaching processes [100,101]. For this purpose the statistics of on-/off- intervals on different timescales (from ns to hours) is investigated depending on various external parameters (temperature, external fields, atmosphere, pressure, etc.).

The technique of blinking statistics analysis is not free of artefacts, for example the dependence of obtained results on the threshold choice [123]. The way to solve this problem is by using the analysis of photon statistics (photon distribution functions, PDF) of single emitters [124–127]. The analysis of the PDF gives relaxation time constants, parameters of intermolecular interaction, spectral diffusion characteristics, etc. This approach is especially productive for the analysis of SM emission at room temperatures, when processes are very fast and spectra are usually structureless. Regarding ultrafast processes, techniques have recently been developed with up to femtosecond temporal resolution [62].

3.2.5 SM luminescence microscopy (imaging)

Initially SM imaging was realised using a scanning confocal microscope with a very sensitive low-noise single channel detector (photomultiplier tube or avalanche photodiode). It was understood that the analysis of a SM image allows reconstruction of the lateral position of a molecule with very high precision, which is not restricted by the diffraction limit, but depends only on the stability of the setup, the precision of scanning module and the signal-to-noise ratio of detected image. Since the development of matrix detectors, especially highly sensitive CCD-cameras with internal electronic multiplication, classical wide-field luminescence microscopy became the basis for numerous SMS investigations and a number of super-resolution microscopy techniques. Moreover, modern technologies allow performing all-3D microscopy of SMs by instrumental modification of their point-spread function.

3.3 Experimental schemes

A general view of a measurement system for various SMSM experiments is presented on Figure 2. In the most advanced configuration, the setup includes implementations of all the spectroscopic techniques discussed above.

In the case of cryogenic measurements, a sample holder is placed into the measuring chamber of the optical (liquid nitrogen or helium) cryostat together with a translation stage and focusing optics. Focusing optics are microscope objectives, with a numerical aperture that is as high as possible ($NA \sim 0.8{-}0.9$, and >1 for the immersion objectives). The translation stage ideally should permit precise control of 3D-translation of the sample relative to the microscope objective. A sample holder unit can be equipped with different elements for implementing various microscopic techniques, for example joined together with a head of atomic-force or scanned-tunnelling microscope, with optical tweezers.

The light source block consists of a laser (e.g. CW tunable narrowband laser) and an excitation preparation unit. The excitation preparation unit fulfils several different functions:

- control of the laser intensity stability with a noise-eater, based on the feed-back Pokkels cell, or a liquid crystal modulator;
- control of the laser frequency stability using a Fabry-Perot interferometer, Michelson interferometer and/or iodine cell;
- defocusing of a light beam for the wide field epi-fluorescence microscopy;
- preparation of on-demand polarized light for polarization spectroscopy;
- preparation of the homogeneous Gaussian light-wave front by spatial pin-hole filter;
- preparation of specially constructed light-wave fronts by spatial amplitude and phase light modulator, e.g. for effective excitation of SM with dominantly axial orientation of transition dipole moment.

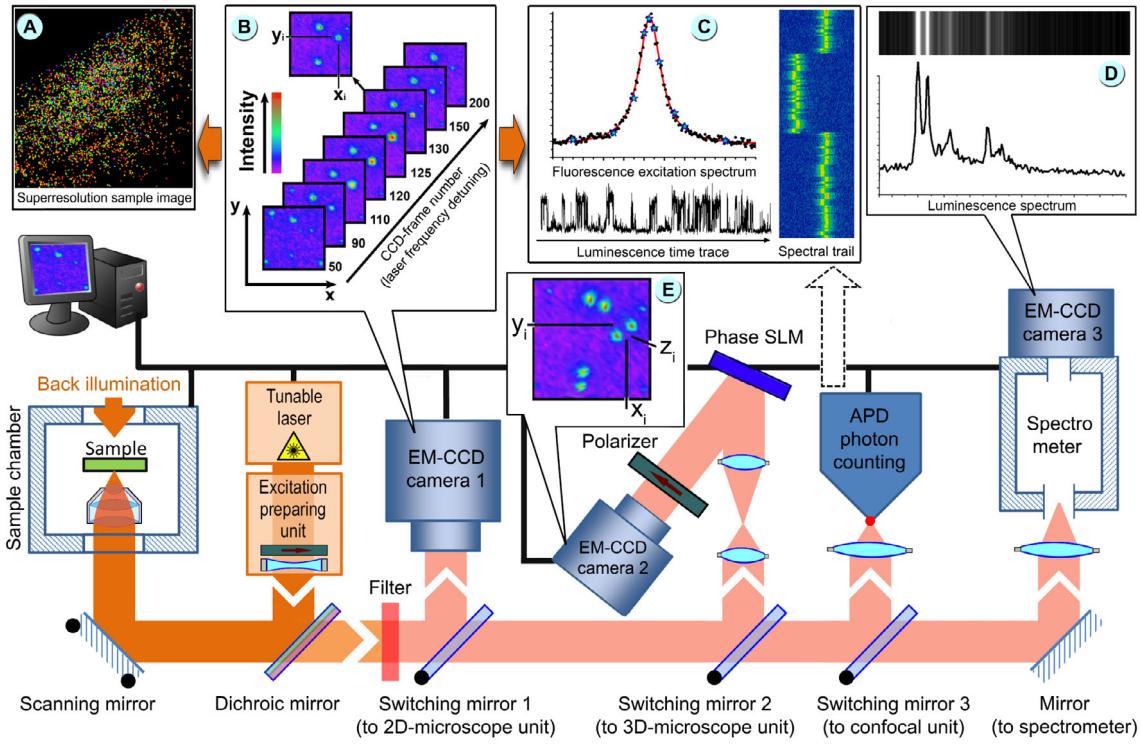

Fig. 2. The principal scheme of a measurement system for single-molecule spectromicroscopy in the most advanced configuration which includes wide-field 2D- and 3D-luminescence microscopes, a scanning confocal microscope, and an imaging spectrometer (see captions and description in the text).

Dichroic mirrors and filters are used for the best separation of detectable emission from the excitation and scattering light. In modern experiments, one usually use the interference filters with very sharp edges. The spectral characteristics are chosen according to the spectral properties of the sample under study.

Figure 2 shows the majority of detection scheme types which are described below. Each scheme can be switched on and off by the corresponding switching mirror.

3.3.1 2D-microscopy unit

Highly sensitive matrix detector camera 1 (fast low-noise CCD-camera with internal electronic multiplication) is used for wide field luminescence microscopy. The fluorescent microscope, either of the epifluorescence design, or with the illumination of a sample from the back-side, allows SM imaging as well as fluorescence excitation spectra measurements (Fig. 2B). The latter is possible by stepped frequency tuning of the narrowband laser.

Both SM imaging and fluorescence-excitation spectra measurements allow super-resolution reconstruction of sample structure (Fig. 2A) by restoring the lateral coordinates of an emitter via computer analysis of a SM image (see details in [18,21,22]). The required molecule density can be achieved by either non-correlated switching of SMs between dark and bright states, or by selective narrowband laser excitation (as illustrated on Fig. 1).

In SM imaging mode, at a fixed excitation wavelength, the SM luminescence time trace and corresponding photon distribution function can be measured (Fig. 2C).

In fluorescence excitation mode, the CCD-camera frame is recorded with certain exposure on each laser frequency detuning step (see Figs. 2B and 2C). After scanning through the whole selected spectral range, the sequence of CCD-frames can be analysed with special image processing software in order to recognise individual images of SMs and extract a fluorescence excitation spectrum for each SM (Fig. 2C). This measurement can be carried out repeatedly in order to detect so called SM spectral trails which reflect dynamical processes in local matrix surroundings (Fig. 2C).

3.3.2 3D-microscopy unit

Recent advances in adaptive optics technologies give the possibility for generating light beam with highly controllable spatial amplitudes and phase modifications. On this basis several techniques for 3D SMs spatial coordinates reconstruction have been developed, e.g. DHPSF [68,112] and BSPPSF [69]. The luminescence from SMs is transformed by a liquid-crystal spatial light phase modulator (SLM) loaded with a specially calculated phase mask. The mask can be also prepared by grey-level lithography of polymer film that is much more photon-efficient [128].

In the case of the DHPSF-technique the SM emission wavefront is modified so that each SM image is "split" into two lobes (Fig. 2E) then detected by CCD-camera 2. The slope of the line connecting two image lobes is related to the axial coordinate (depth) of SM. Thus, high precision reconstruction of both lateral and axial coordinates of a SM can be realised and used for further 3D-super-resolution microscopy of doped samples.

3.3.3 Confocal microscope unit

This unit consists of the single-channel photon counting scheme based on an avalanche photodiode detector. It is the most popular scheme for SMS because it achieves the highest temporal resolution possible for direct SM emission photon counting. Such a scheme is used to detect the SM photon correlation function, luminescence time trace (Fig. 2C) and photon distribution function. A confocal microscope can be used also for the detection of an individual SM fluorescence excitation spectrum and its spectral trail (Fig. 2C).

3.3.4 Imaging spectrometer

This unit is used for the detection of luminescence (or resonance Raman, or enhanced Raman) spectrum of a selected SM (Fig. 2D). As this unit is equipped with a highly sensitive CCD-camera 3, it allows parallel detection of several SMs in imaging mode.

The whole setup is operated with a specially developed computer program which is used for the control of setup units, data acquisition and preliminary processing. In order to ensure the best results, software should be suitable for on-flight SM images recognition and data visualisation. Further statistical data post-processing is a task that is more generally related to the basic topic of "big data analysis".

3.4 Sub-diffraction resolution in far-field single-molecule techniques

SMs are point-like light sources considerably smaller than the wavelength of emitted electromagnetic waves. It means that with apriori knowledge of the point spread function (radiation pattern), one can reconstruct the coordinates of the emitter with an accuracy which is not restricted by the diffraction limit of far field optics but depends on the stability of the experimental setup and the signal-to-noise ratio of the detected signal. For this one needs to perform computer analysis of the SM image detected with a 2D matrix detector (or with a highly precise scanning confocal microscope). As it was shown in early papers [64], the accuracy of lateral coordinates measured for most bright molecules can reach a few nanometers, while the longitudinal coordinate can reach ∼100 nm. The latest studies show that the accuracy of determining coordinates of an emitting centre can reach values below 1 nm [65].

The precise localisation of single emitters is one of the keystones of SMSM and related applications [129]. In many cases one define the SM localisation precision by semi-phenomenological formula [130]:

$$\sigma = \sqrt{\left(\frac{\Gamma_{\mathrm{PSF}}^2 + a^2/12}{N}\right)\left(\frac{16}{9} + \frac{8\pi\Gamma_{\mathrm{PSF}}^2 f_0^2}{a^2 N}\right)}, \qquad (11)$$

where N – the number of collected photons, a – is the pixel size of the imaging detector, f_0 – is the average background signal, Γ_{PSF} – is the standard deviation of PSF. With typical setup parameters it gives precision of ∼10 nm with detection of 1000–2000 photocounts per SM. For bright ZPL SM image such a number of photocounts can be obtained with exposure time of a few tens of milliseconds (at non-saturating laser excitation power).

To achieve the sub-diffraction accuracy of SM coordinates determination, it is necessary to take into account the PSF. In the first approximation, we can consider an individual fluorophore as a point emitter with an ideal radiation pattern (emitting into 4π steradian). In this case, the luminescence SM image is an Airy disc (Fig. 3a), and lateral coordinates are determined by calculating (in the simplest case) the "the centre of gravity" of the molecule image distributed over some CCD-detector pixels (Fig. 3c1). This centroid-approximation is most used in supper-resolution techniques because of the simplicity of image processing.

The next step is a 2D-Gaussian approximation, when the registered luminescence intensity distribution within the SM image is fitted by the two-dimensional Gaussian function. In the simplest case it can be symmetrical (equal width in both x-, y-directions):

$$f(x,y) = f_0 + \frac{A}{\Gamma_{\mathrm{PSF}}}\exp\left(-\frac{(x-x_c)^2}{\Gamma_{\mathrm{PSF}}^2}\right)\exp\left(-\frac{(y-y_c)^2}{\Gamma_{\mathrm{PSF}}^2}\right), \qquad (12)$$

where f_0 is a noise pedestal including the detector noise, parasitic illuminations, nonresonantly excited fluorescence, etc.; A is the signal amplitude; Γ_{PSF} is the PSF width; and x_c and y_c are the lateral SM coordinates (Fig. 3c2).

On Figures 3c1 and 3c2 we illustrate the analysis of the luminescence image of a single organic (tetra-tert-butylterrylene, TBT) molecule in a polymer film at $T = 4.3$ K with excitation at laser wavelength ∼575 nm. The relative lateral coordinates of the molecule can be calculated by finding the "centre of gravity" of the image: $x_c = 22.3$ μm, $y_c = 32.3$ μm (Fig. 3c1). Determination of the lateral coordinates of the same SM by approximating the phononless luminescence image by the 2D-Gaussian function (Eq. (12)) gives $x_c = 22.24 \pm 0.04$ μm; $y_c = 32.35 \pm 0.03$ μm (Fig. 3c2). The analysis of SM image by its fitting with 2D-Gaussian function increases markedly the stability and precision of the procedure of coordinates calculation. Moreover 2D-Gaussian analysis simplifies and automates the localisation procedure.

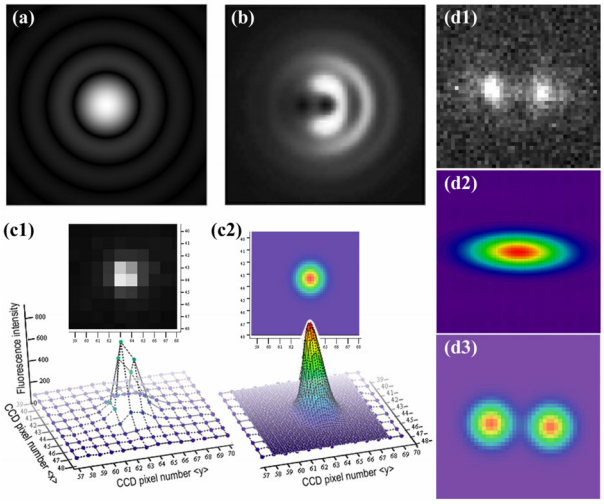

Fig. 3. Illustration of the procedure of analysis of SM point spread function. (a) Airy disk, which corresponds to the PSF of an ideal point light source. The central part of the image is well approximated by a symmetrical 2D-Gauss function. (b) PSF in the emitting dipole approximation: fluorescent images of a single emitting center with the dipole transition moment orientation with 60° angle with respect to the optical axis of the luminescence microscope (taken from [65]). (c1) Typical fluorescent image of a single TBT molecule in a PIB film observed upon resonance ZPL excitation at 4.3 K. (c2) Determination of the lateral coordinates of the same SM by approximating the phononless luminescence image by 2D-Gaussian function (Eq. (12)). (d1) The luminescence image of a single semiconductor quantum dot (QD) CdSe/ZnS (size ∼5 nm) obtained in our recent experiments with the DHPSF single-molecule imaging technique. (d2) Image corresponded to elliptical 2D-Gaussian (Eq. (13)) which can be used for the preliminary localization of DHPSF SM image. (d3) Determination of all three coordinates of the QD by approximation of the image (d1) by a sum of two identical 2D-Gaussian functions (Eq. (12)).

A more accurate analysis requires taking into account the changes in PSF due to a non-in-plane electronic transition dipole moment (Fig. 3b) [65]. Finally, SM luminescence images should be analysed taking into account the PSF changes for SMs near the interface of media with different refractive indices. Also, the PSF can be instrumentally modified in order to realise super-resolution on all 3 coordinates, e.g. with the techniques of DHPSF [68,112] or BSPPSF [69]. In this case the PSF gathers a complicated shape (Fig. 3d1) that complicates image processing. As a result, in the general case, image analysis is more complicated, because the SM image can split into two lobes, became asymmetric, rotated, etc. Image processing in this case requires much more complicated (than 2D-Gaussian fitting) numerical analysis. In some cases the two-dimensional elliptical Gaussian function is very useful for image processing:

$$f(x,y) = f_0 + A\,\exp\Big[-\Big(a\,(x-x_0)^2 + 2b\,(x-x_0) \times (y-y_0) + c\,(y-y_0)^2\Big)\Big], \quad (13)$$

with the coefficients

$$a = \frac{\cos^2\theta}{2\Gamma_x^2} + \frac{\sin^2\theta}{2\Gamma_y^2}, \qquad b = -\frac{\sin 2\theta}{4\Gamma_x^2} + \frac{\sin 2\theta}{4\Gamma_y^2},$$
$$c = \frac{\sin^2\theta}{2\Gamma_x^2} + \frac{\cos^2\theta}{2\Gamma_y^2},$$

where f_0 is a noise pedestal; A is the signal amplitude; Γ_x and Γ_y is the 2D-peak widths in orthogonal directions; x_c and y_c are the lateral coordinates of the center of the lobe; and the rotation of the lobe is defined by clockwise angle θ (for counterclockwise rotation invert the signs in the b coefficient). Such a 2D elliptical Gaussian function is often used in image processing and in computational models of artificial visual systems.

SM image processing procedure in general consists of several stages: noise reduction, single emitter image preliminary localisation, fitting of image with specific PSF, and if possible a further "proof of confidence" (e.g. by time-trace or hyperspectral analysis). For each particular case, specific algorithms and software are usually developed, but several powerful open-source libraries also exist which can be used [110–112].

3.5 Three-dimensional single-molecule microscopy with the technique of double-helix point-spread function

An instrumental modification of the SM emission light beams allows the design of a PSF suitable for reconstruction of all 3 spatial coordinates of the emitter (within reasonable vicinity of the focal plane of microscope objective). The specific engineering of SM PSF is achieved by the transformation of SM emitted light by a phase mask, calculated with the computer procedure of Gauss-Laguerre modes manipulation [131,132]. The first effective application of this idea to SM imaging was realised in [68] by using a double-helix PSF. The phase mask modifies SM emission light beams in such a way that the SM image splits into two lobes, for which the rotation angle depends on the depth of SM position relative to the focal plane of microscope objective.

On Figure 3d1 we show as an example a DHPSF image measured in our recent experiments for a single semiconductor quantum dot (QD) CdSe/ZnS (size ∼5 nm) on a glass substrate. The experiment was performed with a specially developed epi-fluorescence wide-field microscope coupled with an atomic-force microscope (Nano Scan Technology, Russia) at ambient conditions. Fluorescence was excited by a CW laser Coherent Verdi V6 at wavelength 532 nm and was detected with a highly sensitive CCD-camera (PCO Sensicam EM). The calculated phase mask was loaded into the liquid-crystal phase spatial light modulator (Holoeye Pluto BB). Computer analysis of this DHPSF image includes, at first, the single emitter localisation with elliptical 2D-Gaussian (Eq. (13), Fig. 3d2), which also allows initial parameters for further fitting to be found, and then, approximation of the image by the

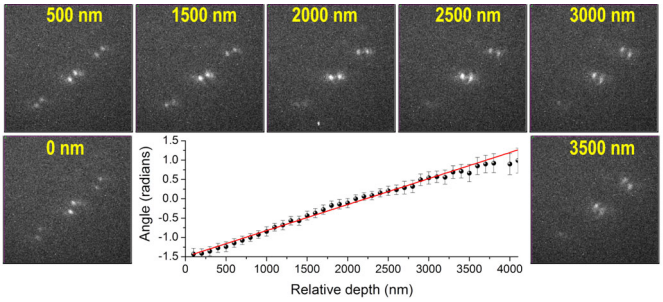

Fig. 4. Luminescence images of three single semiconductor quantum dots CdSe/ZnS on glass substrate depending on the distance to microscope objective focal plane. The DHPSF calibration curve is shown, as obtained by the analysis of images of QD images in the center of the frame.

sum of two identical 2D-Gaussian functions (Eq. (12), Fig. 3d3). With sufficient signal-to-noise ratio, all three coordinates can be reconstructed with sub-diffraction accuracy. For example the single quantum dot image on Figure 3d1 gave lateral coordinates determined with ∼30 nm accuracy, and axial one with ∼80 nm accuracy.

The piezo drive translation stage of the microscope allows precise sample movement in relation to the microscope objective (Fig. 4). Taking into account the high luminescence quantum yield of QDs, the DHPSF scheme can be accurately calibrated. After obtaining the DHPSF calibration curve, all-3D microscopy of single emitters can be realised. One can see from Figure 4, that with the described setup elements a sample thickness appropriate for 3D-diagnostics is ∼4 μm. After such a calibration of the DHPSF-scheme, the setup is ready for 3D-SMSM measurements.

The impressive possibilities of DHPSF SMS technique were demonstrated in a series of recent works [68,112,128] on applications of 3D reconstruction microscopy on biological substances labelled with chromophores at ambient conditions.

The applications of DHPSF techniques with detection of phononless luminescence (SM ZPL) at low temperatures is likely to be very useful in material sciences, as we will show below in Section 5.

4 Low-temperature dynamics of disordered solids

4.1 Manifestation of internal dynamics of matrix in SM spectral trails

Disordered solids like molecular glasses and polymers are characterised by the lack of atomic or molecular long-range ordering. This does not disturb the macroscopic uniformity of the density (or existence of long wave phonon as in crystals) but at the same time results in local microscopic inhomogeneity. The latter brings into existence some outstanding physical phenomena and more complex low-temperature dynamics in comparison with pure crystal media. These physical peculiarities are manifested in "anomalous" temperature dependences of heat capacity and thermal conductivity of disordered solids in comparison with crystals. For example, at cryogenic temperatures, the temperature dependence of thermal conductivity of disordered solids shows a plateau at around ten degrees Kelvin, region and a so-called Boson peak appears in the low-frequency vibration spectrum. According to current concepts of low-temperature dynamics of disordered solids (at temperatures far below glass-transition), such behaviours are mainly caused by a few types of low-energy elementary excitations. These excitations occupy the lowest energy levels on a multidimensional potential hypersurface of a disordered medium. Random distribution of barrier parameters lead to potential surface subdivision into localised regions, which create basic potential shapes for low energy excitations. As a result, low energy excitations appear in one-, two- or rarely, multi-well potentials [87,89,92,133–137].

For single-well potentials vibration excitations can appear as localised or quasi-localised low-frequency mode vibration excitations (LFM). For double-well potentials, there can by tunnelling two level systems (TLS) and thermally activated two-level systems (the so called relaxation systems with overbarrier transitions between two lowest energy levels). Tunnelling TLSs dominate in the temperature range below a few degree Kelvin. This determines low-temperature dynamics and effects in this range. Vibration excitations begin to dominate at higher temperatures and determine dynamical processes above 3−5 K.

Local electric or elastic strain fields in the host matrix result in SM 0-0 transition frequency modifications. Therefore valuable information about local dynamical processes and structural peculiarities are contained in the parameters of SM ZPL: ZPL linewidths, spectral positions, spectral dynamics rates and frequency shift amplitudes (see Sect. 2.6). Interaction with low-energy excitations leads to homogeneous spectral line broadening (optical dephasing) and to 0-0 frequency modification with time (spectral diffusion). The time range available for such measurements is from microseconds (or even nanoseconds) up to several hours.

Since its first days, SMSM has found numerous applications in the study of low-temperature local dynamics of solids and continues to be widely used at present [14–19].

To date, three main types of SM ZPL spectral dynamics at low temperatures have been revealed, which are typical for dye-doped matrices with different degrees of order:

(i) Stable ZPL with absence of any sign of spectral diffusion (Fig. 5a). Such behaviour was observed only in highly ordered molecular crystals [138].
(ii) ZPL discrete jumps between 2^N stable spectral positions (Fig. 5b) which are satisfactorily described within standard tunnelling TLS and stochastic sudden jump models, where N is a number of "slow" (comparing with laser scanning rate) flipping tunnelling TLSs. Interaction of SMs with "fast" TLSs causes a splitting of SM spectrum which is stable in time. Note that observable ZPL jumps/splitting (i.e. large in comparison with ZPL homogeneous linewidth) are caused by TLSs located in close

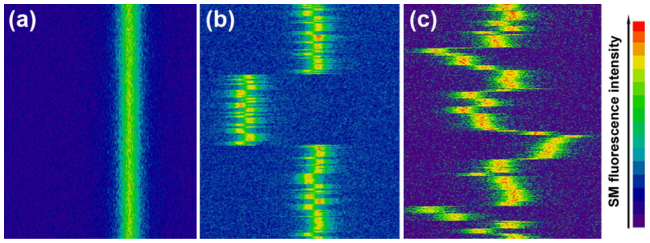

Fig. 5. Three types of ZPL spectral dynamics typical for impurity/matrices with different degrees of order: (a) Terrylene in polycrystalline 1,2-ortho-dichlorobenzene. (b) TBT in amorphous high molecular weight polyisobutylene. (c) TBT in low-molecular weight organic glass (frozen toluene). $T = 7$ K for all three experiments (taken from [139]).

proximity to the SM. The SM interaction with an ensemble of "weak" TLSs (distant located or weakly interacting) leads to small frequency shifts within the SM homogeneous linewidth, i.e. contribute to the observed ZPL broadening. Furthermore, line broadening can be induced by interaction with very fast flipping TLSs when frequency shifts are smaller than the TLS flipping rates. Such ZPL evolution was observed in the many SMS-experiments that have been performed so far [14–19]. In reference [139] such temporal behaviour was found to be mostly typical for high molecular weight polymers.

(iii) Sophisticated spectral dynamics of SM ZPL (Fig. 5c): discontinuous jumps between large numbers of spectral positions and quasi-continual spectral drifts. In a series of experimental works, such behaviour was found to be typical for low-molecular weight glasses, oligomers and ultrathin (a few nanometres) polymeric films [139]. It can arise from interaction with huge number of TLSs, TLS-TLS interaction and from structural relaxations [137].

4.2 Temperature and external field effects

Modification of external electrical field, pressure, variation of temperature and polarisation of excitation laser allow expansion of experimental capabilities of SMSM.

Investigations of the Stark effect in SM systems [14] make it possible to determine the individual dipole moments of SMs, and use such "calibrated" SMs as very sensitive nanoprobes of local electric fields. For example in some cases it allows clarification of the nature of TLS-SM interactions (electrical or elastic dipole-dipole interaction). For example, in reference [97] the value of electric dipole moment of the active TLS was measured.

The experiments wherein SM luminescence intensity is measured with different excitation light polarisation give information about the SM electronic transition dipole moment (Eq. (9)). It can be used for investigation of rotating dynamics near the glass transition temperature at SM level [140]. At low temperatures SM rotations are quenched, and therefore the dipole moment direction is a

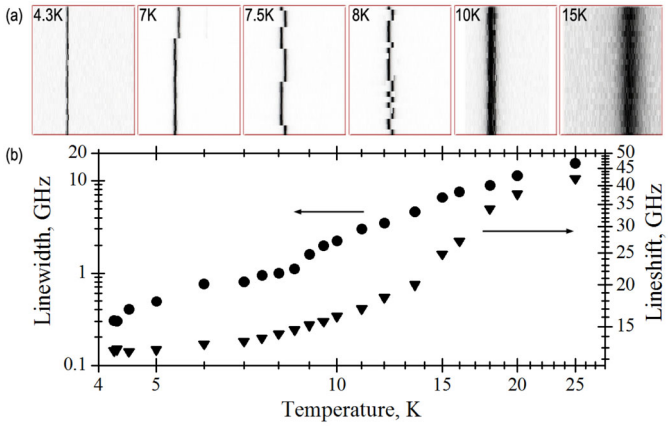

Fig. 6. (a) An example of SM spectral behavior at different temperatures. (b) The temperature dependences of homogeneous ZPL width and shift for the selected SM TBT in PIB (taken from [142]).

good SM identifier [14,94]. For example, polarisation dependence in combination with SM coordinates were used as criteria for identification of the same SM measured before and after heating in a thermocycle [141], and for interpretation of complex SM fluorescence excitation spectra that consisted of several peaks [94].

Finally, temperature is a key parameter for low-temperature dynamics investigation with SMS. With raising temperature, ZPLs become broader, and spectral dynamics become faster and more complex (see Sect. 2.6 and Fig. 6). Temperature variations lead to changes in TLSs flipping rates and corresponding SM spectral dynamics. Figure 6a shows an example of ZPL spectral behaviours of the same SM measured at different temperatures [142]. It was a stable ZPL at 4 K (at least during experimental time), but at 7−7.5 K it began jumping between two positions because of "activation" of a nearby TLS. The jump rate became faster with increasing temperature (8 K) and also linewidth became significantly broader because of electron-phonon interactions (10−15 K). The lower part of Figure 6 shows the temperature dependences of ZPL width and frequency shift for this SM.

4.3 Probing of single low-energy excitations and local structural relaxations

SMS gives a unique opportunity for the measurement of single low-energy excitation parameters. Tunnelling TLS energy splitting, LFM effective local frequencies, and relaxation activation energies can be evaluated from analysis of the ZPL spectral and temporal behaviour at different temperatures, by analysing Stark spectral shifts, and by applying thermal cycles.

The investigation of temperature and temporal dependences of ZPL parameters (Fig. 6) allows determination of the tunnelling TLS energy splitting by analysis of intensity ratio for split SM spectral lines: the ratio of intensities of peaks in split SM spectrum is equal to the ratio of average

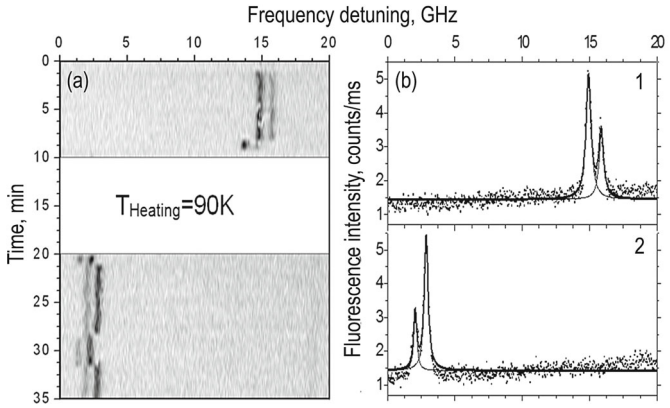

Fig. 7. (a) Spectral behavior of SM TBT in PIB measured at 4.5 K before (20 scans, 10 min) and after (30 scans 15 min) heating in thermal cycle with heating temperature 90 K (b) corresponding spectra summarised on 10 scans: 1 – before heating, 2 – after heating. The intensity ratio of the doublet lines changed under heating in a thermal cycle (taken from [141]).

time that the TLS spends in the upper and lower energy state, which in turn is equal to the Boltzmann exponents for the TLS energies.

Moreover, observation and analysis of split SM spectra, together with thermal cycles, gives a very promising method for investigation of TLS double-well potential modifications and analysis of single thermally activated relaxation system. We will demonstrate this technique on an example taken from reference [141].

Figure 7a shows the spectral behaviour of TBT SM in PIB measured at 4.5 K before (20 scans, 10 min) and after heating (30 scans 15 min) in a thermal cycle with a heating temperature of 90 K. Spectral doublet rarely jumps between the two positions. Figure 7b shows the corresponding spectra (before-1 and after-2 heating) summarised over 10 scans. It is obvious that intensity ratio of the two signals in the doublet was changed under heating in the thermal cycle, which in turn implicates a change in TLS energy and double-well potential asymmetry. It enables us to draw a conclusion about the value of the relaxation system activation energy and its effect on the tunnelling TLS.

Temperature dependences of SM linewidths in the region above 4−5 K can be used for determination of LFM parameters (effective LFM frequency and coupling constant). Electron-phonon interaction of SM with vibration excitations leads to homogeneous line broadening and ZPL spectral shift (Fig. 6b). SM linewidth broadening due to the quadratic electron-phonon coupling can be described in general by equation (6). In the case of interactions between SM and LFM ensembles, this expression is simplified to:

$$\Delta\Gamma_{\mathrm{LFM}}(T) = \sum_j B_j \frac{\exp(-h\nu_j/kT)}{[1-\exp(-h\nu_j/kT)]^2}, \qquad (14)$$

ν_j is the frequency of the LFM with index j, and B_j is a coefficient which denotes the strength of the quadratic electron-phonon interaction of this LFM with a SM. SM linewidth temperature dependence analysis allows us to determine characteristic (efficient) frequency and the interaction strength constant. As was shown in reference [143] vibration dynamics have a localised character and temperature dependences can be fitted in most cases by just one summed term (with one frequency) in equation (14), thus confirming the strong local character of LFM.

4.4 Statistical analysis of SMS-data for study of low-temperature dynamics of disordered solids

SMSM connects the rare local events in doped solids (as tested by one SM-probe) with macroscopic dynamical properties due to the highly parallel detection of luminescence from many separated SMs with a wide-field microscope. For this, various statistical regularities were investigated in the spectra of numerous SMs [15,16,18,21,75]. The distributions of various spectral parameters of SMs were measured and calculated: SM ZPL spectral widths, moments and cumulants of SM spectra, SM transition dipole moments, efficiency of the structural relaxations, etc. Each distribution contains information about a certain property of the bulk sample, revealing its microscopic nature.

For example, the measurement and analysis of T-dependencies of ZPL spectral widths for a large number of SM spatially distributed in a sample allows us to obtain local vibration frequencies in the sample, to find the LFM energy spectrum and compare it with the density of states as measured by inelastic neutron scattering [143,144]. Thereby the possibility to measure a macroscopic characteristic of the sample (density of vibrational states) was demonstrated. Secondly, in the direct experiment, it was shown that vibrational excitations responsible for the ZPL broadening are also responsible for the appearance of Boson peak in glasses. Finally, one of the key questions of impurity centre spectroscopy was clarified, that doping of disordered solids with certain chromophore probe molecules does not change the vibrational dynamics markedly.

5 Luminescent spectromicroscopy of myriad single molecules

5.1 Photophysics of fluorophores: from single emitter to bulk sample

SMS has opened an opportunity of direct measurements of the core photophysical characteristics of fluorescent organic molecules: absorption cross section, fluorescence quantum yield, frequency of molecular vibrations, energy

levels structure, intersystem crossing parameters, dipole moment value and orientation, natural (excited state lifetime limited) linewidth, blinking parameters and mechanisms. As discussed above, the influence of a single emitter's surroundings on its photophysics could be also directly quantified.

An important question in this context is the relationship between the data obtained via SMS "on the microscopic level" – a set of local parameters of a solid matrix – and the macroscopic photophysical characteristics of the whole bulk sample. The solution to this problem is the statistical analysis of individual spectral parameters of many SMs (see, e.g., references [16,18,21,75] and references therein). The combination of SMS and statistical data analysis yields the challenge of linking the distributions of spectral positions, widths, and other characteristics of SM lines (which are determined by the local structure and dynamics) with some macroscopic properties of the solid matrix involved. Significantly more detailed information can be obtained by simultaneous measurements of the spectra and spatial coordinates of SMs. In order to implement this approach, it is necessary to perform parallel measurements of large numbers of SM spectra using a SM luminescence microscope. Up to very recently, however, the number of SM spectra an experimentalist could measure and evaluate was too low to perform accurate statistical analyses.

It was not until the extension of SMSM to cover *all effectively emitting* single molecules [21,22] (shortly *all*-SMSM) that it became possible to extend SM studies to macroscopically large numbers of SM lines comparable with the total number of chromophores in the bulk sample, and finally make a "bridge" between accidental rare events detected by SM probes and general properties of the solid matrix. Description of the setup and the technique, which allow experimentalists to measure fluorescence excitation spectra of all effectively emitting SMs across the whole inhomogeneous absorption band and located within the observed area of a bulk sample at cryogenic temperatures were given in [21,22]. Also in Section 3 of this Colloquium, we presented the principal scheme (Fig. 2) of multifunction setup, which has a unit for epiluminescence 2D-microscopy that can be used for the measurements under discussion. An essential component of the measuring system for the realisation of *all*-SMSM technique is a tunable, narrowband, single-frequency, single-mode laser with the possibility of continuous tuning of the excitation radiation frequency along the whole inhomogeneous absorption band of the sample under investigation. In references [21,22] these conditions were met by a tunable, single-mode ring dye laser Coherent CR699-21 with auto-scan controller, which can perform successive scans with precise stacking over 10 GHz intervals, in the text below referred to as scan segments $\Delta\tilde{\nu}$. As a result of the measurements and initial data processing for each sample under study, a giant set of experimental data was obtained which comprise individual ZPL parameters and spatial coordinates of all detected SMs. The following multivariant statistical analysis enabled us to perform different types of nanodiagnostics (*nanotomography*) of the sample, including, e.g., the calculation of averages, finding different spectral-spatial correlations, etc. Below, several most interesting results obtained with the implementations of *all*-SMSM will be demonstrated.

5.2 Synthetic distributions of single-molecule parameters

An extreme advantage of *all*-SMSM is the possibility for post-experimental construction of various *synthetic distributions of SM parameters* which have different physical meanings. In principle, one can "model" the conditions of any "classical" ensemble averaging technique and perform in-depth comparative analysis. Thereby, many new aspects of bulk sample spectra formation can be investigated.

For example, when dye doped systems are studied by *all*-SMSM, with many options for different statistical distributions, of primary interest are relationships between individual SM ZPL parameters and their spectral positions in the inhomogeneous absorption band (i.e. SM ZPL frequency) of the sample involved. To this end, the following specific statistical analysis procedure was performed in references [21,22]. The entire spectral range within which SM spectra were recorded was divided into small equal spectral intervals (segments) of the width $\Delta\tilde{\nu} = 10$ GHz. The width of a segment determines the averaging interval, and may be larger or smaller depending on the specific task. In this case, the width of a segment $\Delta\tilde{\nu} = 10$ GHz has the same value as a single scan performed by a tunable laser with an auto-scan controller.

For data processing, the following parameters were calculated for each segment:

$\tilde{\nu}$, wave number at the beginning of the segment;

N_{SM}, number of SMs recorded within the segment;

$$\bar{\gamma} = \frac{1}{N_{\mathrm{SM}}} \sum_{i=1}^{N_{\mathrm{SM}}} \gamma_i, \tag{15}$$

average linewidth of the SM spectra in the segment;

$$\bar{I}_{\max} = \frac{1}{N_{\mathrm{SM}}} \sum_{i=1}^{N_{\mathrm{SM}}} (I_{\max})_i \tag{16}$$

average maximum fluorescence count rate;

$$A_{\mathrm{sum}} = \sum_{i=1}^{N_{\mathrm{SM}}} A_i, \tag{17}$$

integral fluorescence from all SMs recognized in the segment.

Besides the calculation of the rather trivial dependences $\bar{\gamma}(\tilde{\nu})$ and $\bar{I}_{\max}(\tilde{\nu})$, which represent the averaged values of the SM spectral linewidths and maximum fluorescence count rates respectively, as a function of the spectral position $\tilde{\nu}$ within the inhomogeneous profile, in references [21,22] several more sophisticated spectral

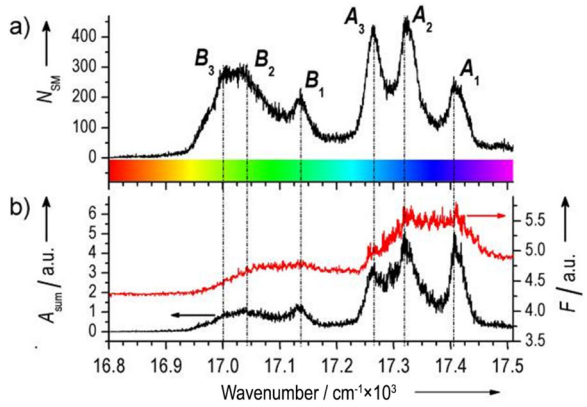

Fig. 8. (a) Spectral density of SMs. (b) Phononless absorption band (black line, scale on the left side) obtained from evaluation of individual spectral parameters of 286 931 terrylene molecules in 1,2-dichlorobenzene measured at $T = 1.5$ K. Fluorescence excitation spectrum (red line, scale on the right side). The vertical dash-dotted lines indicate the frequency positions of resolved sites labeled A1-A3 and B1-B3 in (a). The rainbow scale at the bottom of (a) is used for color encoding of the spectral positions of SMs on Figure 9 (taken with changes from [22]).

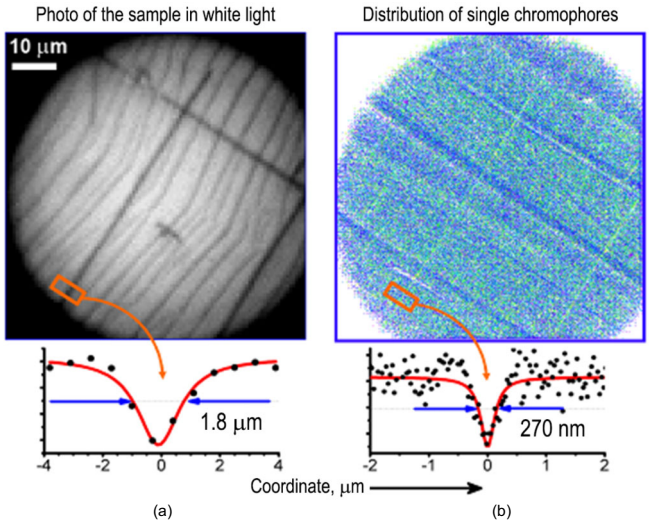

Fig. 9. (a) Photo of the sample of Tr/o-DCB under white-light illumination from the back. (sub-a) Determination of the width of a crack by a Lorentz fit to the transmittance curve obtained from the microscope image. (b) Spatial distribution of the fluorescence images of 286 931 single molecules in the sample. Each SM is depicted by a dot. The color indicates the spectral position within the inhomogeneous band (see rainbow scale on Fig. 8). (sub-b) Determination of the same crack width by a Lorentz fit of curve representing the spatial distribution of SMs along a line perpendicular to the crack (taken from [22]).

"functions" were determined – *the spectral density of SMs* $N_{\rm SM}(\tilde{\nu})$ and *the phononless absorption band* $A_{\rm sum}(\tilde{\nu})$. $N_{\rm SM}(\tilde{\nu})$ denotes the number of SMs detected in the segment with spectral position $\tilde{\nu}$. Thus, it represents the distribution of the ZPL frequencies within the inhomogeneous absorption band. $N_{\rm SM}(\tilde{\nu})$ is related, but not equal, to the high-resolution fluorescence excitation spectrum of a bulk sample, as measured by conventional laser spectroscopy. The differences are due to the fact that the widths, areas, and even shapes of individual SM spectra can be very different, and the distributions of their parameters across the inhomogeneous band may be quite non-uniform. $A_{\rm sum}(\tilde{\nu})$ is also related to the macroscopic high-resolution fluorescence excitation spectrum. It is the frequency dependence of the sum of integrated ZPLs for all SMs registered within a segment. Thus, $A_{\rm sum}(\tilde{\nu})$ is not completely equivalent to the fluorescence excitation spectrum of a bulk sample either: The important difference is that $A_{\rm sum}(\tilde{\nu})$ does not contain the PSBs of the chromophores.

Figure 8 shows the distributions $N_{\rm SM}(\tilde{\nu})$ and $A_{\rm sum}(\tilde{\nu})$ obtained in references [21,22] from evaluation of individual spectral parameters of 286 931 SMs measured at low temperature in an o-dichlorobenzene (o-DCB) matrix doped with terrylene (Tr) molecules (taken with changes from [22]). The inhomogeneous absorption band of Tr/o-DCB has a quasi-site structure, which is best resolved in the spectral density $N_{\rm SM}(\tilde{\nu})$ (Fig. 8a). At least six different spectral sites were observed (A_1-A_3, B_1-B_3). For comparison, the red curve overlaid in Figure 8b shows the usual fluorescence-excitation spectrum of the selected sample area, $F(\tilde{\nu})$, which is structureless, because it includes the contributions from non-resonantly excited molecules. Such an unstructured inhomogeneous band can be calculated as the sum of a set of spectral sub-bands [121], composed of the narrow ZPLs within $\Delta\tilde{\nu}$ and corresponding broad PSBs.

5.3 Multicolour super-resolution microscopy of doped solids

The possibility of sequential-parallel separate detection of a huge number of SM ZPLs within the whole inhomogeneous absorption band, followed by reconstruction of SM spatial coordinates with nanometre accuracy, allows us to achieve the spatial density of registered SMs within a diffraction limited volume that is high enough for far-field nanodiagnostics of extended objects. For this, in reference [22] individual ZPL parameters were measured along with super-precision reconstruction of lateral coordinates for each of the 286 931 terrylene SMs. This huge number of dopant fluorophores separately imaged in a sample volume with dimensions $70\times70\times0.5$ μm corresponds to a labelling density of ∼35 molecules per diffraction limited volume of the sample, which is sufficient for super-resolution diagnostics of extended objects. To illustrate this, we show on Figure 9 the main result of nanodiagnostics from reference [22]. Figure 9a shows a microscopic photograph of the Tr/o-DCB sample under back-side illumination with white light. The polycrystalline structure of the sample is clearly visible. Consideration of one of the cracks on the white-light microscopy image yields a diffraction limited width of about 1.8 μm for this structure (Fig. 9(sub-a)).

Another situation takes place in the case of phononless optical reconstruction single-molecule spectromicroscopy. Figure 9b shows the 2D image of the positions of all 286 931 recorded SMs in the sample plane. The lateral coordinates of each SM was obtained by calculation of its image centroid. Each fluorophore is represented by a dot, whose colour corresponds to the rainbow spectrum encoding the ZPL frequencies at the bottom of Figure 8a. The heterogeneities in the spatial distribution of SMs near the cracks are clearly visible on Figure 9b. The bright straight lines indicate the lower density of fluorophores inside the cracks. From the spatial distribution of the fluorescence SM images, the width of this crack is determined as 270 ± 50 nm, i.e. overcoming the diffraction limit (Fig. 9(sub-b)).

If one observes the structure of straight line cracks on the sample photo under white-light illumination on Figure 9a and compares them to the SM spatial distribution in Figure 9b, it can be concluded that for one of the cracks, the SM density is clearly higher on one side of it than on the other (dark blue line in Fig. 9b). One of the possible reasons is that local (e.g. strain) fields cause an anisotropic migration of the fluorophores toward the crack during freezing. Another interesting peculiarity is that lines of higher SM density running parallel to the crack are visible in at least three other locations (Fig. 9b), for which the photograph does not show any cracks at that places. It is probable that these lines of higher SM density are the manifestations of strong local inhomogeneity or strain fields along one of the crystallographic axes, at which cracks can, but do not necessarily, develop during crystallisation. Along the perpendicular cracks, the inhomogeneities of the SM density are qualitatively different – there is no sign of SM density increase along these cracks.

5.4 Spectral-spatial nanodiagnostics of solids

One of the well-known advantages of impurity centre spectroscopy is that the electronic spectra of dye centres embedded into a solid matrix are very sensitive to their local surroundings, and contain valuable information about structure and dynamics in the nearby neighbourhood. The neighbourhood is different for different impurity centres, and one of the main "difference parameters" is the spatial position of a centre in the host matrix. Thus, to study and discuss the differences in spectra and spectral dynamics of dopants, while gathering no information about their spatial positions in a sample structure, would mean loosing sight of the most important physical relationship in this type of spectroscopy. SMSM technique gives at the output both spectral characteristics and spatial coordinates of recorded impurity centres. Thus, it becomes possible to investigate many aspects of this physical relationship by analysing various correlations between spectral properties of SMs and their spatial positions within a sample structure. In this paragraph, we show examples of such *spectral-spatial analyses*.

In reference [94], the first attempt to match the directions of SM transition dipole moments with the matrix structure was performed on the example of typical Shpol'skii matrix, *n*-hexadecane (*n*-Hex) doped with terrylene molecules. For this, the authors performed polarisation spectroscopy experiments (see Sect. 2.6 and Eq. (9) of the present Colloquium). It allows reconstructing the orientations of SM dipole moments projections on a sample plane. At the same time, SM imaging gives lateral spatial coordinates for all observed SMs. Thus, SM dipole moment direction can be analysed in relation to SM position within a sample structure (Fig. 10). From observing the distributions of SM dipole moment orientations, the authors found that in the system under study, different sample structures exist: crystals with preferred orientation, samples with domains of aligned crystals, and samples where crystals were mixed at random. They concluded that the resulting microstructure of the Shpol'skii matrix under study could not be predetermined and varies from sample to sample.

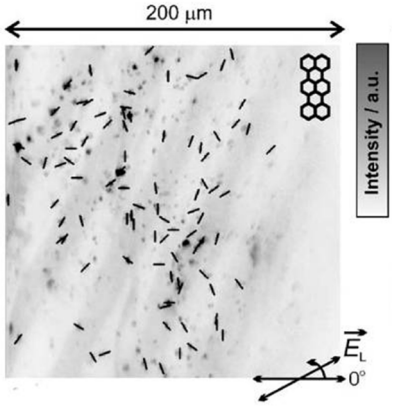

Fig. 10. An image of fluorescing sample (Tr/*n*-Hex) with an inverted intensity scale. For each SM, its dipole moment orientation is overplotted on the fluorescence sample image as a black stretch. The direction of the rotation of the vector $\mathbf{E_L}$ (polarization) is counted from the horizontal axis (taken from [94]).

The potential of *all*-SMSM may be revealed most pronouncedly in synchronous analysis of spectral parameters and spatial coordinates of *myriad* SMs. Such an analysis opens up the way to gain deeper insight into the nature of structural and photophysical features of a sample.

In reference [21], Tr/*n*-Hex system was investigated with the implementation of *all*-SMSM by recording ZPLs and lateral coordinates for a huge number (105 332) of SMs. Among many other impressive results, an attempt to look inside the microscopic nature of a spectral site and its relation to the sample structure has been made. Namely, the main site S_1 of the inhomogeneous absorption band of Tr/*n*-Hex was specially considered. On Figure 11a the spectral density of Tr molecules in *n*-Hex at $T = 1.5$ K measured in [21] is plotted by a solid black line. The main spectral site S_1 of this system is well resolved. It had always been assumed in previous studies that this spectral site corresponds to a unique incorporation of the Tr molecule in the *n*-Hex matrix.

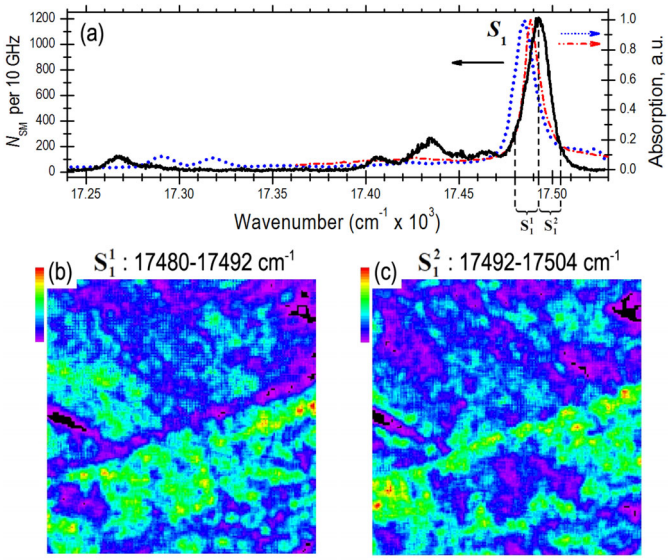

Fig. 11. (a) Spectral density of Tr molecules in polycrystalline *n*-Hex at $T = 1.5$ K as measured in reference [21] (*solid black line, left axis*); absorption (fluorescence excitation) spectra for Tr/*n*-Hex as obtained by conventional spectroscopy for bulk sample in [145] (*dash-dot red line, right axis*) and in [146] (*dot blue line, right axis*). (b,c) Colour-encoded topograms representing the spatial density of SMs with different spectral positions in the sample plane in the spectral region of main site S_1: Parts (b) and (c) correspond to ZPLs in the spectral interval 17 480–17 492 cm^{-1} and 17 492−17 504 cm^{-1}, respectively. The spatial density reaches values of up to ∼200 molecules per μm^3 (*red colour in the topograms*) (taken from [21]).

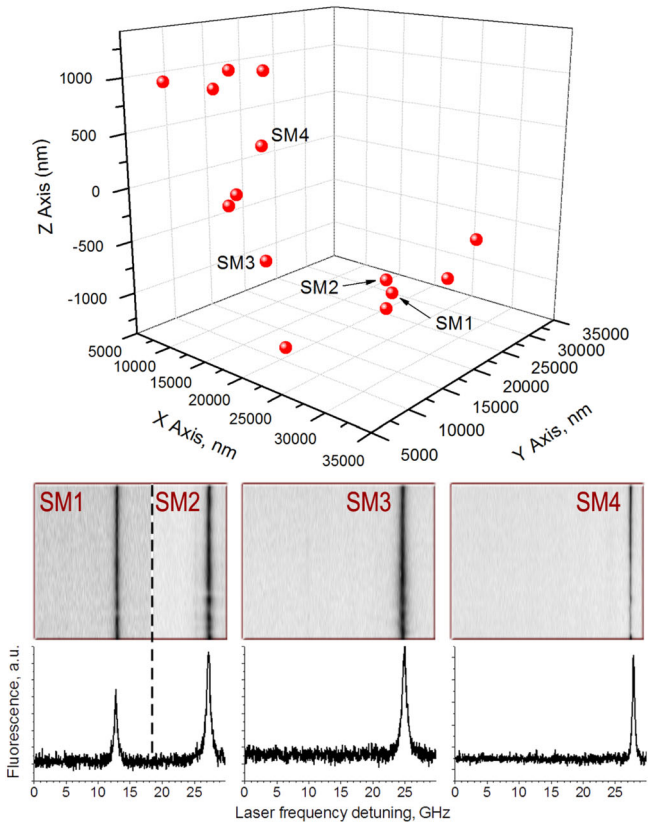

Fig. 12. 3D-mapping of 14 single Tr molecules in o-DCB film, as measured by detection of their ZPLs and phononless luminescence images by DHPSF technique. On the middle panels, the SM spectral trails of four selected SMs. Bottom panel shows the corresponding fluorescence excitation spectra.

In reference [21], the spatial (lateral) distribution of the SMs forming the site S_1 was calculated. It was a big surprise to find that that these SMs can be roughly divided into two groups. Figures 11b and 11c show the spatial density of Tr molecules whose spectra are located in the low-frequency (Fig. 11b) and the high-frequency wing of S_1 (Fig. 11c), respectively. Both SM spatial distributions correspond to identical structures in the polycrystalline sample, but they show a pronounced anti-correlation with each other. This can be ascribed to the presence of a sub-site structure of peak S_1, which had never been discussed so far. A possible interpretation is that the *n*-Hex crystal provides two slightly different ways for the Tr molecules incorporation. A clarification of this assumption may be performed with the help of crystallographic calculations.

5.5 Double-helix point spread function phononless luminescence SMSM

The above discussed achievements of *all*-SMSM lead us to the development of a technique for 3D (with reconstruction of all the spatial coordinates) hyperspectral nanodiagnostics of solids on the base of phononless luminescence single-molecule spectromicroscopy with modification of SM PSF by the double-helix scheme.

Here we present the first results of SM ZPL and spectral trails detection in the system terrylene in polycrystalline 1,2-ortho-dichlorobenzene at $T = 5$ K. For the measurements, we built the setup based on the epi-luminescence microscope scheme, and included a tunable dye-laser Coherent CR-699, optical cryostat RTI (Russia) with temperature control system Lakeshore 93C, and the cryogenic micro-objective Microthec $NA = 0.8$, CCD-camera PCO Sensicam EM. DHPSF-mode spectroscopy was realised and calibrated as described in Section 3.4. The laser was tuned within a 30 GHz range by scanning 1000 discrete steps; the exposition was 200 ms per point. In total, 31 scans were performed. As a result, we have succeeded in measurements of three spatial coordinates, fluorescence excitation spectra and spectral trails for a number of molecules in the sample under study (Fig. 12).

Thereby we demonstrate the possibility to perform phononless luminescence 3D-spectromicroscopy of single molecules in solids.

6 Problems and open questions

In this section, we briefly specify the main technical problems and some open questions in the field of

spectromicroscopy of myriad single molecules, including the subfield of low temperatures:

(a) Deep understanding of intra- and inter- molecular interactions (energy transfer, electron-phonon coupling, electron-tunnelling coupling, intersystem crossing, Auger-ionisation, photo-oxidation, photo-induced conformation changes), nature of blinking and bleaching.
(b) Development of highly stable and remote controllable sample mounts, 3D-translation stages and optics, which are operable at different conditions (including cryogenic temperatures). The technique becomes even more powerful and informative when SMSM is combined with other instruments, like AFM, STM, optical tweezers, Raman spectrometers, high pressure chambers, magnetic field chambers, optical cryostats, etc. Such instruments are very complicated but already on the way to becoming widespread (see examples in Ref. [147]).
(c) Development of the methods for highly effective excitation of single emitters, for example with specific excitation light wave fronts preparation [96], with fluorescence enhancement by nanoantennas [83–86], etc.
(d) The methods of sample preparation with high (sub-ppm) purity.
(e) Development of the methods for theoretical calculation and synthesis of new luminescent molecules and nano-objects (semiconductor or dielectric quantum dots, single ions in nanocrystals, hybrid nano-objects, molecular and biological complexes) with desired or controllable photophysical properties such as luminescence quantum yield, absorption band, capability to ZPL emission, switching, broadening, spectral diffusion (see e.g. [119,148,149]).
(f) Image processing (various point-spread functions, high level of background signal and noises, uncontrolled impurities in a sample, separation of single emitters and agglomerates, control of setup mechanical instability, fast algorithms) [110–112].
(g) Big data processing (statistical analysis of massive spectral-spatial data). Similarly to the approaches used in astrophysics [150,151], SMSM has come to the stage when a large open source-distributed database can be created, which will contain complete experimental information about photophysical properties of various impurity solids in the form of spectromicroscopic data about all efficiently-emitting single impurity centres in macroscopic volumes of various materials. This will make possible realisation of the "data mining" concept, thus combining the efforts of many specialists in the processing of giant volumes of information, development of the methods for analysing this information, searching for fundamental regularities, development of the corresponding models and theories.

7 Conclusions

Concluding this Colloquium paper, one needs to say that spectromicroscopy of single molecules is a start-up technique for a broad field of multidisciplinary basic research and applications. The methods of SMSM become especially powerful and informative when myriad single-molecules are detected, and when measurements are performed at low temperatures suitable for observation of narrow zero-phonon spectral lines (which ultrasensitive to local environment structure and dynamics).

At present, it is possible to measure low-temperature fluorescence excitation spectra and coordinates for the majority of fluorescing SMs in bulk doped solids (crystals, glasses, polymers). For this, specially developed algorithms and software should be applied for quick (real-time) SM spectra and images recognition, data processing and specific statistical analyses. Experimental data postprocessing and numerical analysis give opportunities:

(a) to study comprehensively the photophysical properties of fluorescent media (from single emitter up to bulk sample), in particular to investigate the intermolecular processes, and the phenomena of single quantum objects emission enhancement, bleaching and blinking;
(b) to probe processes in doped solids on the microscopic level (up to single low-energy elementary excitations, single charge carrier transfer); to search and study rare local events; to probe local fields and energy/charge transfer on a microscopic level
(c) to recognise/analyse anomalies and artifacts (e.g. sub-ppm chemical contamination);
(d) to construct synthetic distributions of SM parameters, which have physical meaning, compare them with ensemble averaged data obtained by classic experimental techniques;
(e) to search and analyse the physical nature of various correlations between local parameters of a sample (e.g. spectral-spatial).

We also demonstrate for the first time that phononless single-molecule spectromicroscopy is possible using the scheme of double-helix point spread function, allowing far-field reconstruction of all three spatial coordinates of SMs with nanometre accuracy. Thus, the 3D multicolour super-resolution microscopy of doped solids can be realised.

The developed approach can be implemented for various applications in material sciences related to far-field nanodiagnostics and specific "hyperspectral nanotomography" of solids and surfaces (i.e. visualisation of particular structures and nanoregions of the sample with different local photo-physical and dynamical properties; defects and cracks detection; surface inspection; detection and study of nanoparticles of different nature and chemical composition).

The financial support from Russian Science Foundation (14-12-01415) and Russian Foundation for Basic Researches (14-02-00822) is acknowledged. The authors sincerely thank Yaroslav Sobolev and Sergei Orlov, who contributed to building the setup used in low-temperature DHPSF SMSM measurements described in Section 5.5. (Y.S. has developed the control box software for synchronous operating of tunable

laser and SMSM detection system; S.O. has developed and implemented the cryogenic sample translation stage). The results shown on Figures 5–9 and 11 for illustrations were obtained previously and published in cited articles. The fruitful collaboration with coauthors is cordially acknowledged.

References

1. W.E. Moerner, L. Kador, Phys. Rev. Lett. **62**, 2535 (1989)
2. M. Orrit, J. Bernard, Phys. Rev. Lett. **65**, 2716 (1990)
3. "*Special Issue on Super-Resolution Imaging*" Nat. Photon. **3**, 361 (2009)
4. "*Themed Issue on Single-Molecule Optical Study of Soft and Complex Matter*" Phys. Chem. Chem. Phys. **13**, 1697 (2011)
5. "*Special Issue on Single-Molecule Optical Spectroscopy*" Chem. Soc. Rev. **43**, 963 (2014)
6. "*Special Issue on Single-Molecule Studies*" Chem. Phys. Chem. **13**, 881 (2012)
7. P.J.S. Smith, I. Davis, C.G. Galbraith, A. Stemmer, J. Opt. **15**, 090201 (2013)
8. L. Novotny, B. Hecht, in *Principles of nano-optics* (Cambridge University Press, Cambridge, 2006), p. 539
9. B. Lounis, M. Orrit, Rep. Progr. Phys. **68**, 1129 (2005)
10. A. Beveratos, S. Kuhn, R. Brouri, T. Gacoin, J.P. Poizat, P. Grangier, Eur. Phys. J. D **18**, 191 (2002)
11. Q.S. Wei, H.F. Qi, W. Luo, D. Tseng, S.J. Ki, Z. Wan, Z. Gorocs, L.A. Bentolila, T.T. Wu, R. Sun, A. Ozcan, ACS Nano **7**, 9147 (2013)
12. O. Morozova, M.A. Marra, Genomics **92**, 255 (2008)
13. P.S. Dittrich, A. Manz, Nat. Rev. Drug Discov. **5**, 210 (2006)
14. M. Orrit, J. Bernard, R.I. Personov, J. Phys. Chem. **97**, 10256 (1993)
15. T. Basché, W.E. Moerner, M. Orrit, U.P. Wild, in *Single-molecule optical detection, imaging and spectroscopy* (VCH, Weinheim, 1997), p. 250
16. A.V. Naumov, Y.G. Vainer, Phys. Usp. **52**, 298 (2009)
17. M. Orrit, W.E. Moerner, High Resolution Single-Molecule Spectroscopy in Condensed Matter, in *Physics and Chemistry at Low Temperatures*, edited by L. Khriachtchev (Pan Stanford Publishing, Singapore, 2011), pp. 381-417
18. A.V. Naumov, Phys. Usp. **56**, 605 (2013)
19. B. Kozankiewicz, M. Orrit, Chem. Soc. Rev. **43**, 1029 (2014)
20. K.K. Rebane, J. Lumin. **100**, 219 (2002)
21. A.V. Naumov, A.A. Gorshelev, Y.G. Vainer, L. Kador, J. Kohler, Phys. Chem. Chem. Phys. **13**, 1734 (2011)
22. A.V. Naumov, A.A. Gorshelev, Y.G. Vainer, L. Kador, J. Kohler, Angew. Chem. Int. Ed. **48**, 9747 (2009)
23. E.V. Shpol'skii, Sov. Phys. Usp. **3**, 372 (1960)
24. R.H. Silsbee, Phys. Rev. **128**, 1726 (1962)
25. K.K. Rebane, V.V. Khizhnyakov, Opt. Spectrosc. **14**, 362 (1963)
26. E.D. Trifonov, Sov. Phys. Doklady, **7**, 1105 (1963)
27. D.E. McCumber, M.D. Sturge, J. Appl. Phys. **34**, 1682 (1963)
28. M.A. Krivoglaz, Sov. Phys. Solids State **6**, 1340 (1964)
29. K.K. Rebane, Usp. Fiz. Nauk **143**, 487 (1984)
30. M.N. Sapozhnikov, Phys. Stat. Sol. B **75**, 11 (1976)
31. A.A. Maradudin, Theoretical and Experimental Aspects of the Effects of Point Defects and Disorder on the Vibrations of Crystals – 1, in *Solid State Physics*, edited by S. Frederick, T. David, (Academic Press, 1966), Vol. 18, pp. 273-420
32. Y.V. Denisov, V.A. Kizel', Opt. Spectrosc. **23**, 251 (1967)
33. A. Szabo, Phys. Rev. Lett. **25**, 924 (1970)
34. R.I. Personov, E.I. Al'Shits, L.A. Bykovskaya, Opt. Commun. **6**, 169 (1972)
35. R.I. Personov, E.L. Al'shits, L.A. Bykovskaya, J. Exp. Theor. Phys. Lett. **15**, 431 (1972)
36. L. Brus, J. Chem. Phys. **63**, 3123 (1975)
37. B.M. Kharlamov, R.I. Personov, L.A. Bykovskaya, Opt. Commun. **12**, 191 (1974)
38. A.A. Gorokhovskii, R.K. Kaarli, L.A. Rebane, J. Exp. Theor. Phys. Lett. **20**, 216 (1974)
39. A. Renn, U.P. Wild, A. Rebane, J. Phys. Chem. A **106**, 3045 (2002)
40. R.N. Shakhmuratov, A. Rebane, P. Megret, J. Odeurs, Phys. Rev. A **7**, 053811 (2005)
41. S. Volker, Ann. Rev. Phys. Chem. **40**, 499 (1989)
42. J. Kikas, A. Suisalu, A. Kuznetsov, A. Laisaar, J. Takahashi, V. Hizhnyakov, Opt. Spectrosc. **98**, 675 (2005)
43. C. Crepin, N. Shafizadeh, W. Chin, J.P. Galaup, J.G. McCaffrey, S.M. Arabei, Low Temp. Phys. **36**, 451 (2010)
44. S.M. Arabei, T.A. Pavich, K.N. Solovyov, J. Porphyrins and Phthalocyanines **17**, 636 (2013)
45. D.J. Norris, A.L. Efros, M. Rosen, M.G. Bawendi, Phys. Rev. B **53**, 16347 (1996)
46. M.A. Drobizhev, M.N. Sapozhnikov, I.G. Scheblykin, O.P. Varnavsky, M. VanderAuweraer, A.G. Vitukhnovsky, Chem. Phys. **211**, 455 (1996)
47. A.P. Nizovtsev, S.Y. Kilin, F. Jelezko, I. Popa, A. Gruber, J. Wrachtrup, Physica B **340**, 106 (2003)
48. I. Sildos, A. Osvet, Phys. Stat. Sol. A **172**, 15 (1999)
49. S.P. Feofilov, A.A. Kaplyanskii, R.I. Zakharchenya, Y. Sun, K.W. Jang, R.S. Meltzer, Phys. Rev. B **54**, R3690 (1996)
50. Y. Berlin, A. Burin, J. Friedrich, J. Kohler, Phys. Life Rev. **3**, 262 (2006)
51. H.M. Wu, M. Ratsep, I.J. Lee, R.J. Cogdell, G.J. Small, J. Phys. Chem. B **101**, 7654 (1997)
52. R. Kunz, K. Timpmann, J. Southall, R.J. Cogdel, J. Kohler, A. Freiberg, J. Phys. Chem. B **117**, 12020 (2013)
53. F. Ariese, A.N. Bader, C. Gooijer, Trac-Trends Anal. Chem. **27**, 127 (2008)
54. A.B. Myers, P. Tchenio, M.Z. Zgierski, W.E. Moerner, J. Phys. Chem. **98**, 10377 (1994)
55. F. Guttler, T. Irngartinger, T. Plakhotnik, A. Renn, U.P. Wild, Chem. Phys. Lett. **217**, 393 (1994)
56. E. Betzig, R.J. Chichester, Science **262**, 1422 (1993)
57. W.P. Ambrose, P.M. Goodwin, J.C. Martin, R.A. Keller, Phys. Rev. Lett. **72**, 160 (1994)
58. X.S. Xie, R.C. Dunn, Science **265**, 361 (1994)
59. S.M. Nie, D.T. Chiu, R.N. Zare, Science **266**, 1018 (1994)
60. J.J. Macklin, J.K. Trautman, T.D. Harris, L.E. Brus, Science **272**, 255 (1996)
61. S. Weiss, Science **283**, 1676 (1999)
62. R. Hildner, D. Brinks, N.F. van Hulst, Nat. Phys. **7**, 172 (2011)
63. T. Schmidt, G.J. Schutz, W. Baumgartner, H.J. Gruber, H. Schindler, Proc. Natl. Acad. Sci. USA **93**, 2926 (1996)

64. A.M. van Oijen, J. Kohler, J. Schmidt, M. Muller, G.J. Brakenhoff, Chem. Phys. Lett. **292**, 183 (1998)
65. S. Habuchi, S. Onda, M. Vacha, Phys. Chem. Chem. Phys. **13**, 1743 (2011)
66. M.J. Rust, M. Bates, X.W. Zhuang, Nat. Methods **3**, 793 (2006)
67. E. Betzig, G.H. Patterson, R. Sougrat, O.W. Lindwasser, S. Olenych, J.S. Bonifacino, M.W. Davidson, J. Lippincott-Schwartz, H.F. Hess, Science **313**, 1642 (2006)
68. S.R.P. Pavani, M.A. Thompson, J.S. Biteen, S.J. Lord, N. Liu, R.J. Twieg, R. Piestun, W.E. Moerner, Proc. Natl. Acad. Sci. USA **106**, 2995 (2009)
69. A.S. Backer, M.P. Backlund, A.R. von Diezmann, S.J. Sahl, W.E. Moerner, Appl. Phys. Lett. **104**, 193701 (2014)
70. I.S. Osad'ko, Sov. Phys. Sol. Stat. **13**, 974 (1971)
71. D. Hsu, J.L. Skinner, J. Chem. Phys. **81**, 5471 (1984)
72. V. Hizhnyakov, I. Tehver, Chem. Phys. Lett. **422**, 299 (2006)
73. I. Osad'ko, *Selective Spectroscopy of Single Molecules* (Springer, 2010)
74. J.L. Skinner, D. Hsu, Optical Dephasing of Ions and Molecules in Crystals, in *Advances in Chemical Physics* (John Wiley & Sons Inc., 2007), pp. 1-44
75. E. Geva, J.L. Skinner, J. Phys. Chem. B **101**, 8920 (1997)
76. E. Barkai, Y.J. Jung, R. Silbey, Ann. Rev. Phys. Chem. **55**, 457 (2004)
77. P. Borri, W. Langbein, S. Schneider, U. Woggon, R.L. Sellin, D. Ouyang, D. Bimberg, Phys. Rev. Lett. **87**, 157401 (2001)
78. B. Krummheuer, V.M. Axt, T. Kuhn, Phys. Rev. B **65**, 195313 (2002)
79. E.A. Muljarov, R. Zimmermann, Phys. Rev. Lett. **93**, 237401 (2004)
80. C. Lin, I. Renge, R. Jankowiak, Chem. Phys. Lett. **576**, 15 (2013)
81. D.V. Kuznetsov, V.K. Roerich, M.G. Gladush, J. Exp. Theor. Phys. **113**, 647 (2011)
82. M.G. Gladush, D.V. Kuznetsov, V.K. Roerich, Eur. Phys. J. D **64**, 511 (2011)
83. S. Kühn, U. Hakanson, L. Rogobete, V. Sandoghdar, Phys. Rev. Lett. **97**, 017402 (2006)
84. T.H. Taminiau, F.D. Stefani, F.B. Segerink, N.F. Van Hulst, Nat. Photon. **2**, 234 (2008)
85. J.W. Liaw, J.H. Chen, C.S. Chen, M.K. Kuo, Opt. Express **17**, 13532 (2009)
86. A. Kinkhabwala, Z.F. Yu, S.H. Fan, Y. Avlasevich, K. Mullen, W.E. Moerner, Nat. Photon. **3**, 654 (2009)
87. W. Phillips, J. Low Temp. Phys. **7**, 351 (1972)
88. J.R. Klauder, P.W. Anderson, Phys. Rev. **125**, 912 (1962)
89. P.W. Anderson, B.I. Halperin, C.M. Varma, Philos. Mag. **25**, 1 (1972)
90. E. Geva, J.L. Skinner, J. Chem. Phys. **109**, 4920 (1998)
91. B.M. Kharlamov, Opt. Spectrosc. **91**, 461 (2001)
92. U. Buchenau, M. Prager, N. Nücker, A.J. Dianoux, N. Ahmad, W. Phillips, Phys. Rev. B **34**, 5665 (1986)
93. I. Gerhardt, G. Wrigge, P. Bushev, G. Zumofen, M. Agio, R. Pfab, V. Sandoghdar, Phys. Rev. Lett. **98**, 033601 (2007)
94. T.Y. Latychevskaia, A. Renn, U.P. Wild, J. Lumin. **118**, 111 (2006)
95. A.C. Wirtz, M. Dokter, C. Hofmann, E.J.J. Groenen, Chem. Phys. Lett. **417**, 383 (2006)
96. S.V. Boichenko, E.F. Martynovich, J. Exp. Thero. Phys. Lett. **97**, 52 (2013)
97. M. Bauer, L. Kador, J. Lumin. **98**, 75 (2002)
98. M. Bauer, L. Kador, Chem. Phys. Lett. **407**, 450 (2005)
99. A.A.L. Nicolet, M.A. Kol'chenko, C. Hofmann, B. Kozankiewicz, M. Orrit, Phys. Chem. Chem. Phys. **15**, 4415 (2013)
100. J. Schuster, F. Cichos, C. von Borczyskowski, Opt. Spectrosc. **98**, 712 (2005)
101. S.V. Orlov, A.V. Naumov, Y.G. Vainer, L. Kador, J. Chem. Phys. **137**, 194903 (2012)
102. J. Schuster, J. Brabandt, C. von Borczyskowski, J. Lumin. **127**, 224 (2007)
103. F. Cichos, C. von Borczyskowski, M. Orrit, Curr. Opin. Colloid Interface Sci. **12**, 272 (2007)
104. M.A. Kol'chenko, B. Kozankiewicz, A. Nicolet, M. Orrit, Opt. Spectrosc. **98**, 681 (2005)
105. H.R. Petty, Microscopy Res. Tech. **70**, 687 (2007)
106. Z.L. Huang, H.Y. Zhu, F. Long, H.Q. Ma, L.S. Qin, Y.F. Liu, J.P. Ding, Z.H. Zhang, Q.M. Luo, S.Q. Zeng, Opt. Express, **19**, 19156 (2011)
107. T. Hinohara, Y.I. Hamada, I. Nakamura, M. Matsushita, S. Fujiyoshi, Chem. Phys. **419**, 246 (2013)
108. E. Bertin, S. Arnouts, Astron. Astrophys. Suppl. Ser. **117**, 393 (1996)
109. M.H. Yang, D.J. Kriegman, N. Ahuja, IEEE Trans. Pattern Anal. Machine Intell. **24**, 34 (2002)
110. S. Wolter, M. Schüttpelz, M. Tscherepanow, S. Van De Linde, M. Heilemann, M. Sauer, J. Microsc. **237**, 12 (2010)
111. RapidSTORM: an open source evaluation tool for fast and highly configurable data processing for single-molecule localization microscopy, University Wuerzburg, Theodor-Boveri-Institute for Biosciences, Chair of Biotechnology and Biophysics, http://www.super-resolution.biozentrum.uni-wuerzburg.de/home/rapidstorm/ (2012)
112. M.D. Lew, A.R.S. von Diezmann, W.E. Moerner, *Easy-DHPSF open-source software for three-dimensional localization of single molecules with precision beyond the optical diffraction limit*, Protocole Exchange (2013)
113. E. Lang, J. Baier, J. Kohler, J. Microsc. Oxf. **222**, 118 (2006)
114. F. Kulzer, T. Xia, M. Orrit, Chem. Int. Ed. **49**, 854 (2010)
115. T. Zuchner, A.V. Failla, A.J. Meixner, Chem. Int. Ed., **50**, 5274 (2011)
116. W. Gohde, J. Tittel, T. Basche, C. Brauchle, U.C. Fischer, H. Fuchs, Rev. Sci. Instrum. **68**, 2466 (1997)
117. M.A. van Dijk, A.L. Tchebotareva, M. Orrit, M. Lippitz, S. Berciaud, D. Lasne, L. Cognet, B. Lounis, Phys. Chem. Chem. Phys. **8**, 3486 (2006)
118. M. Celebrano, P. Kukura, A. Renn, V. Sandoghdar, Nat. Photon. **5**, 95 (2011)
119. V.S. Lebedev, A.S. Medvedev, Quantum Electron. **43**, 1065 (2013)
120. E.A. Gastilovich, Usp. Fiz. Nauk **161**, 83 (1991)
121. N.L. Naumova, I.A. Vasil'eva, I.S. Osad'ko, A.V. Naumov, Opt. Spectrosc. **98**, 535 (2005)
122. T. Basche, W.E. Moerner, M. Orrit, H. Talon, Phys. Rev. Lett. **69**, 1516 (1992)
123. C.H. Crouch, O. Sauter, X.H. Wu, R. Purcell, C. Querner, M. Drndic, M. Pelton, Nano Lett. **10**, 1692 (2010)

124. L. Fleury, J.M. Segura, G. Zumofen, B. Hecht, U.P. Wild, Phys. Rev. Lett. **84**, 1148 (2000)
125. Y. He, E. Barkai, Phys. Rev. Lett. **93**, 068302 (2004)
126. I. Gopich, A. Szabo, J. Chem. Phys. **122**, 014707 (2005)
127. I.S. Osad'ko, J. Exp. Theor. Phys. **104**, 853 (2007)
128. G. Grover, S. Quirin, C. Fiedler, R. Piestun, Biomed. Opt. Express **2**, 3010 (2011)
129. H. Deschout, F.C. Zanacchi, M. Mlodzianoski, A. Diaspro, J. Bewersdorf, S.T. Hess, K. Braeckmans, Nat. Methods **11**, 253 (2014)
130. K.I. Mortensen, L.S. Churchman, J.A. Spudich, H. Flyvbjerg, Nat. Methods. **7**, 377 (2010)
131. S.N. Khonina, V.V. Kotlyar, V.A. Soifer, M. Honkanen, J. Lautanen, J. Turunen, J. Modern Opt. **46**, 227 (1999)
132. E.G. Abramochkin, V.G. Volostnikov, Phys. Usp. **47**, 1177 (2004)
133. W.A. Phillips, in *Amorphous solids: low-temperature properties* (Springer-Verlag, Berlin, 1981), p. 167
134. V.G. Karpov, M.I. Klinger, F.N. Ignatiev, Zhurnal Eksperimentalnoi I Teoreticheskoi Fiziki **84**, 760 (1983)
135. U. Buchenau, Y.M. Galperin, V.L. Gurevich, D.A. Parshin, M.A. Ramos, H.R. Schober, Phys. Rev. B **46**, 2798 (1992)
136. N.V. Surovtsev, J.A.H. Wiedersich, V.N. Novikov, E. Rossler, A.P. Sokolov, Phys. Rev. B **58**, 14888 (1998)
137. V. Lubchenko, P.G. Wolynes, Annu. Rev. Phys. Chem. **58**, 235 (2007)
138. A.A. Gorshelev, A.V. Naumov, I.Y. Eremchev, Y.G. Vainer, L. Kador, J. Kohler, Chem. Phys. Chem. **11**, 182 (2010)
139. I.Y. Eremchev, Y.G. Vainer, A.V. Naumov, L. Kador, Phys. Chem. Chem. Phys. **13**, 1843 (2011)
140. K. Paeng, L.J. Kaufman, Chem. Soc. Rev. **43**, 977 (2014)
141. I.Y. Eremchev, Y.G. Vainer, A.V. Naumov, L. Kador, Phys. Sol. Stat. **55**, 710 (2013)
142. Y.G. Vainer, A.V. Naumov, M. Bauer, L. Kador, J. Chem. Phys. **122**, 244705 (2005)
143. Y.G. Vainer, A.V. Naumov, M. Bauer, L. Kador, Phys. Rev. Lett. **97**, 185501 (2006)
144. I.Y. Eremchev, A.V. Naumov, Y.G. Vainer, L. Kador, J. Chem. Phys. **130**, 184507 (2009)
145. W. Moerner, T. Plakhotnik, T. Irngartinger, M. Croci, V. Palm, U.P. Wild, J. Phys. Chem. **98**, 7382 (1994)
146. A. Sigl, M. Orrit, T. Reinot, R. Jankowiak, J. Friedrich, J. Chem. Phys. **127**, 084510 (2007)
147. J.V. Chacko, F.C. Zanacchi, A. Diaspro, Cytoskeleton **70**, 729 (2013)
148. Y. Avlasevich, C. Li, K. Mullen, J. Mater. Chem. **20**, 3814 (2010)
149. K.R. Karimullin, A.V. Naumov, J. Lumin. **152**, 15 (2014)
150. D.G. York et al., Astron. J. **120**, 1579 (2000)
151. M.J. Graham, S.G. Djorgovski, A. Mahabal, C. Donalek, A. Drake, G. Longo, Distributed Parallel Databases **30**, 371 (2012)